UNCLASSIFIED

AD NUMBER

AD272404

NEW LIMITATION CHANGE

TO

Approved for public release, distribution unlimited

FROM

Distribution authorized to U.S. Gov't. agencies and their contractors; Administrative/Operational Use; NOV 1961. Other requests shall be referred to Aeronautical Systems Div., Wright-Patterson AFB, OH 45433.

AUTHORITY

AFFDL ltr 21 Oct 1974

THIS PAGE IS UNCLASSIFIED

WADD TECHNICAL NOTE 60-276

SOME RESEARCH EFFORTS RELATED TO PROBLEMS OF AERODYNAMIC DECELERATION

HELMUT . HEINRICH

DEPARTMENT OF AERONAUTICAL ENGINEERING
UNIVERSITY OF MINNESOTA

NOVEMBER 1961

This report is not to be announced
or distributed automatically
in accordance with
AFR 205-43A, paragraph 6d.

AERONAUTICAL SYSTEMS DIVISION

NOTICES

WADD TECHNICAL NOTE 60-276

SOME RESEARCH EFFORTS RELATED TO PROBLEMS OF AERODYNAMIC DECELERATION

HELMUT G. HEINRICH

DEPARTMENT OF AERONAUTICAL ENGINEERING
UNIVERSITY OF MINNESOTA

NOVEMBER 1961

FLIGHT ACCESSORIES LABORATORY
CONTRACT No. AF 33(616)-6372
PROJECT 6065, TASK 60252

AERONAUTICAL SYSTEMS DIVISION
AIR FORCE SYSTEMS COMMAND
UNITED STATES AIR FORCE
WRIGHT-PATTERSON AIR FORCE BASE, OHIO

200 - January 1962 - 16-705

FOREWORD

This report was prepared by the Department of Aeronautical Engineering of the University of Minnesota in compliance with United States Air Force Contract No. AF 33(616)-6372.

The work being accomplished under this contract is sponsored jointly by the O[illegible] Research and Engineering Command, Department of the Army; Bureau of Naval Weapons, Department of the Navy; and Air Research and D[illegible] [illegible]ment Command, Department of the Air Force, a[illegible] is directe[illegible] by a Tri-Service Steering Committee concerned [illegible]th Aerodynamic Retardation. Contract administration is co[illegible]ducted by Wright Air Development Division and Mr. Rudi J. Bern[illegible] of the Aerodynamic Decelerator Branch, Flight Accessories Laboratory, Wright Air Development Division, is Project Engineer.

ABSTRACT

The status of research efforts designed to explain physical phenomena associated with the operation of aerodynamic decelerators, in particular textile type parachutes, is presented. A theoretical approach to calculate the velocity and pressure distribution in the turbulent wake of basic bodies of revolution is outlined and compared to actual test results. The concept of the effective porosity of textile materials is developed, and its influence on the aerodynamic and opening characteristics of conventional textile parachute canopies is discussed. The results of research efforts to reduce parachute inflation time with minor increase of opening force are presented.

PUBLICATION REVIEW

The publication of this report does not constitute approval by the Air Force of the findings or conclusions contained herein. It is published only for the exchange and stimulation of ideas.

FOR THE COMMANDER:

George A. Solt, Jr.
Chief, Aerodynamic Decelerator Branch
Flight Accessories Laboratory

TABLE OF CONTENTS

LIST OF ILLUSTRATIONS

Figure No.		Page

Figure No. | Page

Figure No.		Page

SECTION 1

INTRODUCTION*

The term aerodynamic retardation shall encompass all matters concerning the reduction of the velocity of an airborne object by means of devices whose principal purpose is to produce aerodynamic drag. In this sense, arrangements which produce a retarding force through the conversion of stored energy such as retro-rockets or jet engine thrust reversers shall be excluded from this discussion.

Retardation devices are needed for operation at subsonic as well as at supersonic speeds and, similar to the methods in conventional aerodynamics, one has to pursue research efforts in both principal flow regimes.

In view of the drag per unit of storage volume or weight, the conventional parachute may be considered as a highly efficient device. However, the requirements of stability, reproducibility of performance, and proper functioning at supersonic speed cannot be satisfied with just one efficient type of parachute, and more sophisticated

*This report is based on a presentation before the Wissenschaftliche Gesellschaft fuer Luftfahrt, Hamburg, Germany in 1959.

Manuscript released by the author on 18 October 1960 for publication as a WADD Technical Note.

forms such as flat plates, cones, truncated cones, and spheres have to be considered.

As a design principle, it is desirable to achieve the effective form of the retardation device through self-inflation, which means the rigidity of the drag producing object has to be derived from a careful balance between the pressure distribution on the object and the static equilibrium of the structure of the entirely flexible object. It should be stated that at present this problem has been solved satisfactorily for subsonic but not supersonic velocities.

SECTION 2

THE WAKE EFFECTS

An additional complication arises from the fact that, conventionally, retardation devices are located in the turbulent wake of the suspended load, which shall be called the primary body. The retardation device will be called the secondary body. The ultimate objective for problems of aerodynamic retardation is, of course, the determination of the drag of the system consisting of primary and secondary body. However, the mechanism of the turbulent wake of the primary body alone is already very complicated and, to speak with Schlichting (Ref 1), it is doubtful that a complete understanding of this subject can ever be achieved.

Since for aerodynamic retardation a solution is needed which provides, with a reasonable effort, numerical results, a new attempt is now under way which emphasizes the determination of the total drag of the two-body system. The first step in this analysis is the determination of the velocity distribution of the turbulent wake which is schematically presented in Fig 2-1.

Based on classical relationships by Prandtl and Schlichting, Swain (Ref 2) proposed an equation of motion and derived an equation predicting the local velocity in the turbulent wake, indicated in Fig 2-1. The symbols in the Prandtl-Schlichting relationship, in Swain's equations,

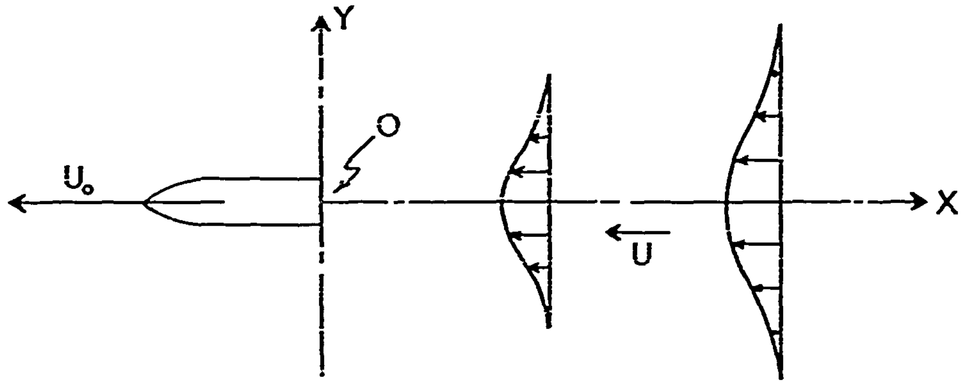

$$L^2\left(\frac{\partial U}{\partial Y}\right)^2 = \varkappa b(U_{max}-U_{min})\frac{\partial U}{\partial Y}\ , \qquad U_0\frac{\partial U}{\partial X} = \frac{1}{Y}\frac{\partial}{\partial Y}\left[L^2 Y\left(\frac{\partial U}{\partial Y}\right)^2\right]$$

(PRANDTL - SCHLICHTING) [illegible]N -1929)

$$U = -U_0\left(\frac{C_D S}{X^2}\right)^{1/2}\left[\frac{(\eta')^{3/2}}{3(3\varkappa^2)^{1/2}} - C_1\right]\ , \qquad U = U_0\frac{A}{X^{2/3}}\cdot e^{-\frac{\eta^2}{6K\varkappa A}}$$

$$\eta' = r\cdot(C_D\cdot S\cdot X)^{-1/3} \qquad \eta = r\cdot x^{-1/3}$$

(SWAIN) (RIABOKIN - HEINRICH -1959)

$$\frac{U}{U_0} = \frac{0.104}{X^{2/3}}\left(\frac{C_D S}{\varkappa^2}\right)^{1/3}\cdot e^{-\frac{r^2}{1.525(C_D\cdot S\cdot X\cdot\varkappa)^{2/3}}}$$

$$S = \pi\frac{D^2}{4} \qquad r^* = \frac{r}{D/2}$$

$$\frac{U}{U_0} = \frac{0.104}{(X/D)^{2/3}}\left(\frac{C_D\pi}{4\varkappa^2}\right)^{1/3}\cdot e^{-\frac{0.413(r^*)^2}{(X/D)^{2/3}\cdot(C_D\cdot\pi\cdot\varkappa)^{2/3}}}$$

FIG 2-1. SCHEMATIC PRESENTATION OF THE VELOCITY DISTRIBUTION OF THE TURBULENT WAKE and in the Heinrich-Riabokin relationships presented in Fig 2-1 are defined as follows:

A, K, η, η'	= Coefficients of proportionality
C_D	= Drag coefficient
C_1	= Constant of integration
D	= Diameter of body of revolution
S	$= \pi D^2/4$
U_o	= Velocity of the undisturbed fluid
U	= Component of velocity in wake
b	= Width of mixing zone of wake
L	= "Mischungsweg" - mixing distance
$\varkappa$	= An empirical constant
X, Y	= Cartesian coordinates
X, r	= Cylindrical coordinates.

In the new approach (Ref 3) an exponential function for the local velocity was postulated which satisfies Swain's equation of motion expressed in terms of Prandtl's basic relationship. The exponential function includes two so far unknown coefficients A and K. If now Swain's solution is considered to be a useful approximation, it can be used for the determination of these unknown coefficients in the new approach. This has been done through the comparison of the drag- momentum relationship expressed in Swain's terms and by means of the exponential function for the local velocity. In this manner one can replace the coefficients A and K by known terms, and the method under Ref 3 derives a relatively simple expression for the velocity distribution.

The application of the new method to actual cases appears to be easier than the older ones, but it remains to be seen how good the new method is. Figure 2-2 shows a comparison between the available analytical and experimental treatments of the subject. One recognizes that the approach in accordance to Ref 3 provides good agreement over a large region of the wake, and deviates from available experimental data merely at the peripheral section. (The term "z" relates the local velocity "U" to the particular velocity, $U = U_{max}/2$, and the radius at which this occurs. For details see Ref 3.)

On the basis of this comparison the new method appears to be useful, and it shall be used for the pursuit of further wake problems, one of which shall be the determination of the pressure distribution in the wake of a primary body consisting of an ogive-cylinder. As the first step in this effort the wake was surveyed; the results of the measurements are shown in Fig 2-3.

From these results one can derive the χ-values used previously in the analytical treatment and one can then compare the experiments with the theory. It is apparent that the χ-value will depend on the L/D position from which it was obtained. Connected herewith is the fact that the quality of approximation derived for one particular χ-value will differ for the various cross sections. An inspection of Figs 2-4 through 2-6 indicates clearly these circumstances.

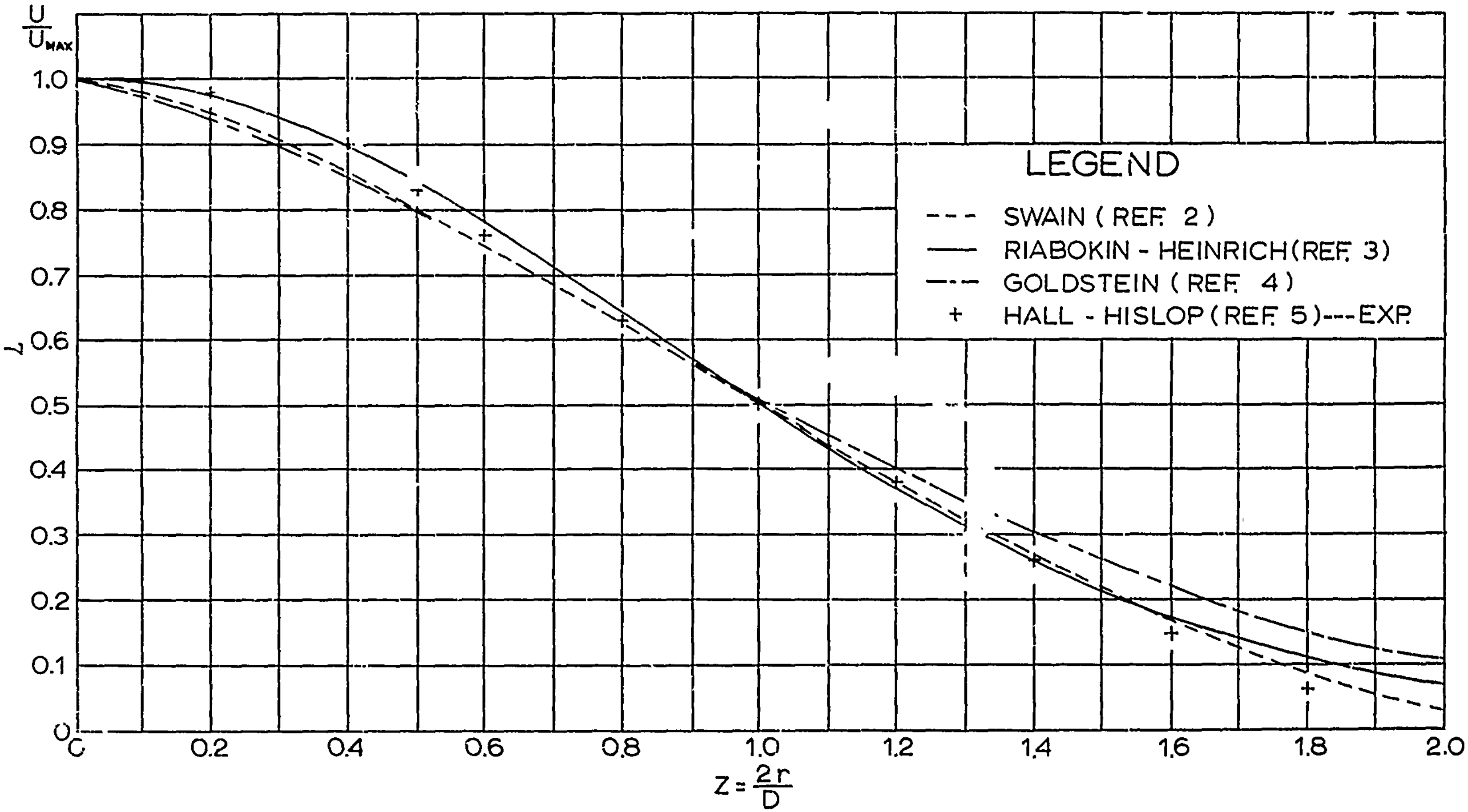

FIG 2-2. VELOCITY DISTRIBUTION IN ACCORDANCE WITH ANALYTICAL AND EXPERIMENTAL STUDIES

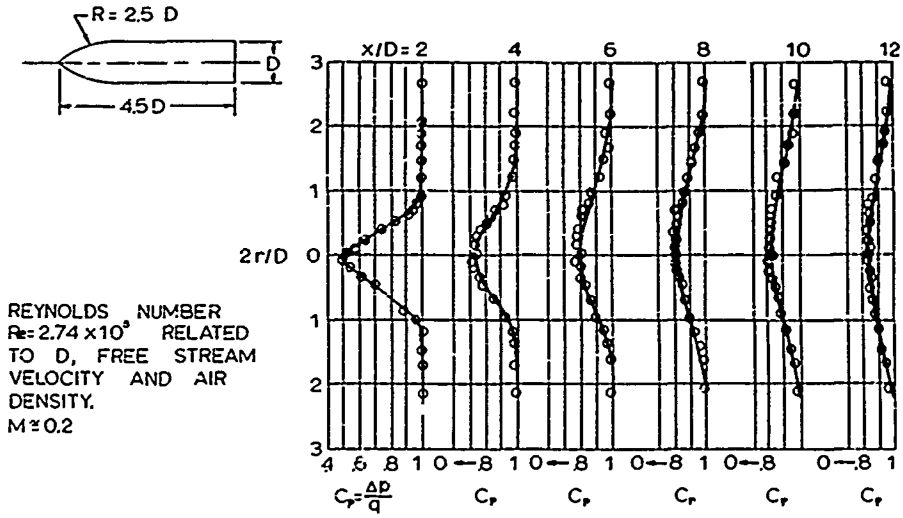

FIG 2-3. EXPERIMENTAL PRESSURE DISTRIBUTION IN THE WAKE OF A BODY OF REVOLUTION
($C_D = 0.35$)

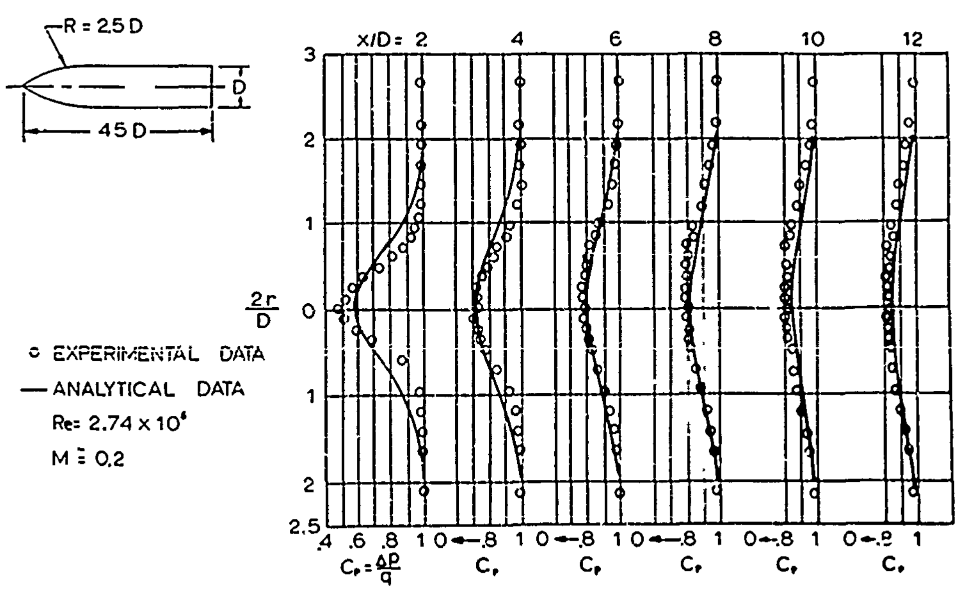

FIG 2-4. EXPERIMENTAL AND ANALYTICAL DATA FOR A BODY OF REVOLUTION
(BASED ON $\chi = 0.0764$ RELATED TO C_p AT $x/D = 4$)

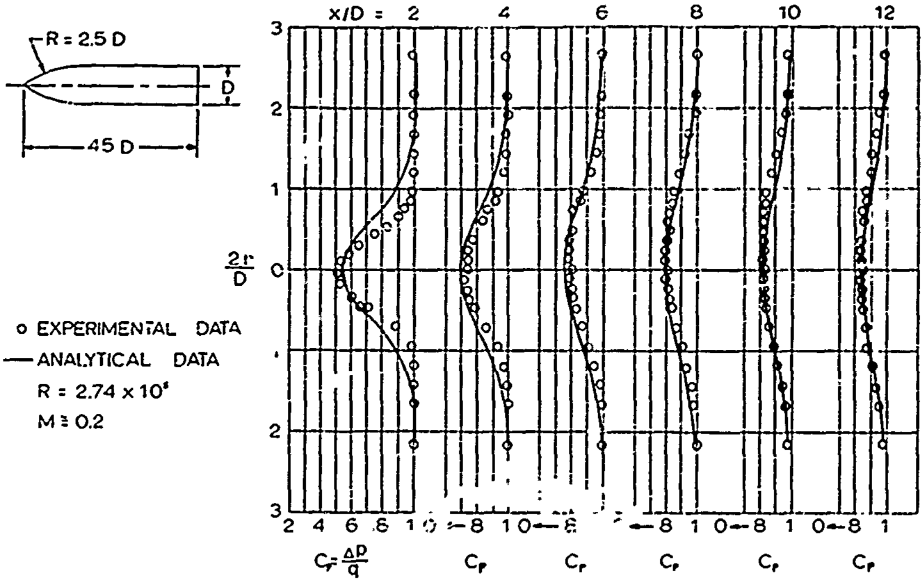

FIG 2-5. EXPERIMENTAL AND ANALYTICAL DATA FOR A BODY OF REVOLUTION
(BASED ON ')0633 RELATED TO C_p AT x/D = 8)

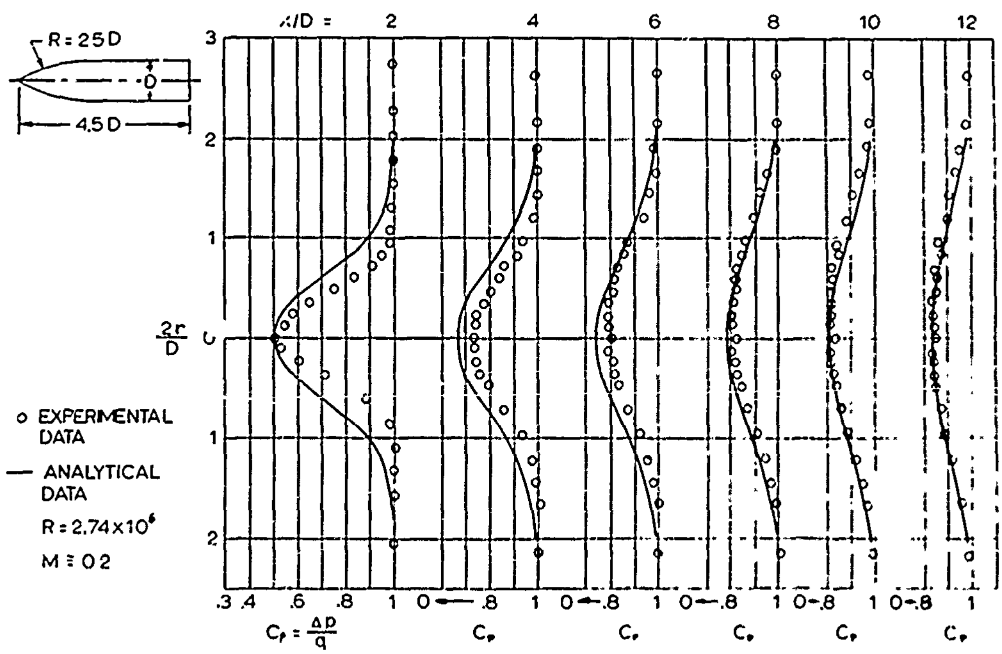

FIG 2-6. EXPERIMENTAL AND ANALYTICAL DATA FOR A BODY OF REVOLUTION (BASED ON χ=.00552 RELATED TO C_p AT X/D=12)

It is significant to note that the pressure on the centerline always can be matched by the theory, while the analytical prediction deviates considerably in the peripheral part, particularly when the control section is relatively close to the base of the primary body.

In Ref 3, certain χ-values as a function of the distance X/D are suggested.

The next step, in view of the prime objective, is the determination of the drag of seco... ...dies located at various positions in the turbu...nt wake. ...nce analytical or semi-analytical approaches are not available at this time, the study m... begin with the ...easurement of the drag of some potential secondary bodies. Fig 2-7 shows the basic secondary bodies under consideration and their free-stream drag coefficients as well as their drag coefficients at various locations behind the primary body. It should be mentioned that in this table the diameter of the primary body is half that of the secondary, and L denotes the distance between the base of the primary and the leading point or plane of the secondary body. Figures 2-8 and 2-9 present graphically the same results.

Attempts are now being made to find a generalization of the relationship of drag to size and location of the primary and secondary bodies, with the total pressure in the centerline of the system as independent variable. Preliminary results are encouraging, but at this time they are not

MODELS	C_D - COEFFICIENT OF DRAG					
	C_{D_∞}	L/D = 2	L/D = 4	L/D = 6	L/D = 8	L/D =10
HEMISPHERE 	1.449	1.242	1.269	1.325	1.374	1.394
SPHERE 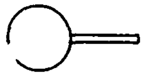	0.105	0.180	0.145	0.141	0.121	0.107
FLAT PLATE 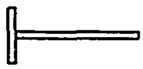	1.143	0.895	1.001	0.986	1.001	0.994
45° CONE 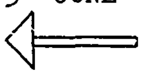	0.702	[illegible]	0.675	0.674	0.675	0.684
30° CONE 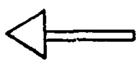	0.530	0.528	0.522	0.518	0.518	0.522
45° TRUNCATED CONE 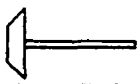	0.727	0.689	0.699	0.705	0.700	0.706

FIG 2-7. DRAG COEFFICIENT OF VARIOUS BODIES IN FREE STREAM AND IN THE WAKE OF A PRIMARY BODY WITH A DRAG COEFFICIENT $C_D = 0.35$; $M = 0.2$, $Re = 2.74 \times 10^5$.

ready for publication.

For the compressible flow regime, similar information is needed. However, its achievement is much more costly and time consuming. Also, the strong effect of Mach number and the variation of the base pressure of the primary body due to the presence of the secondary are further complications.

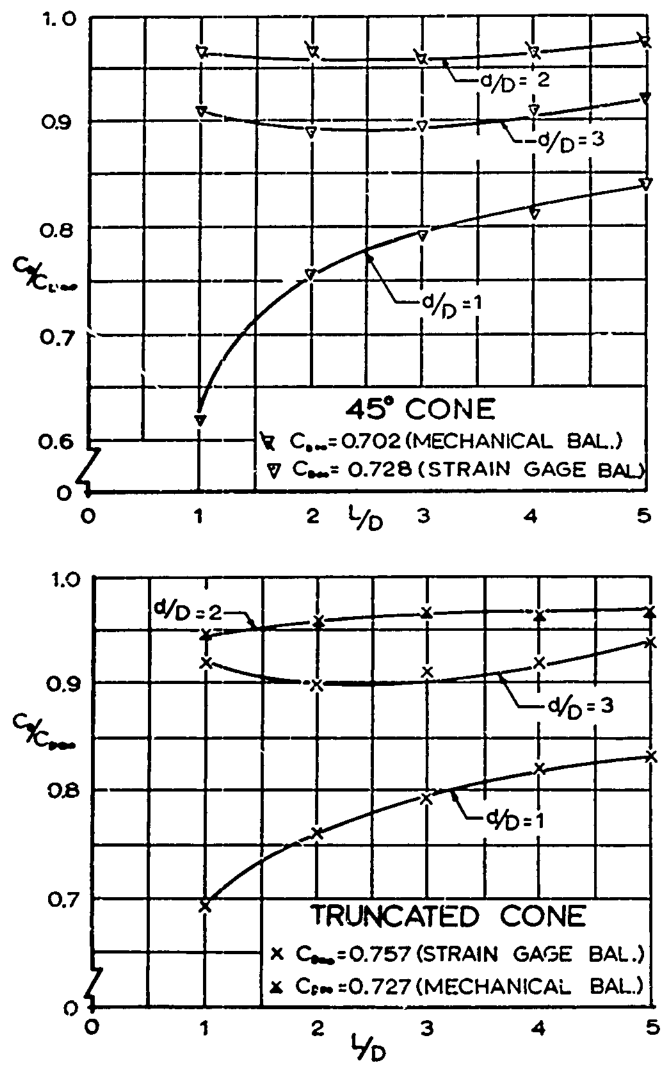

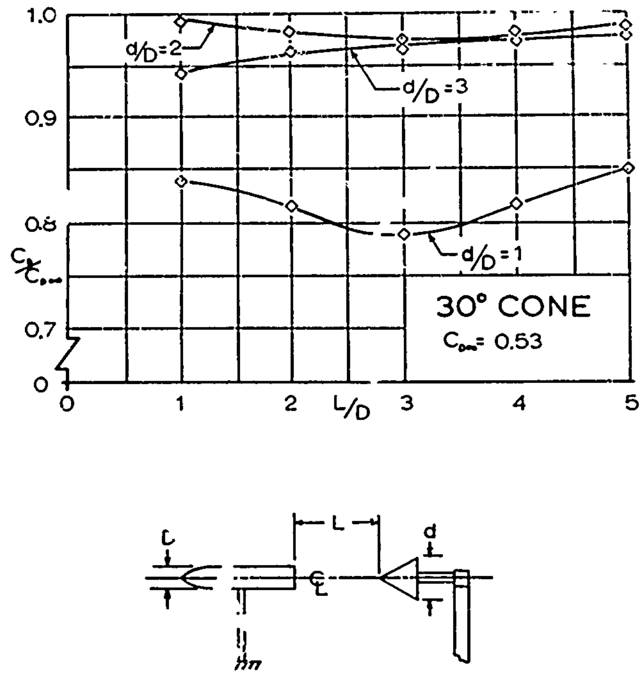

FIG 2-8. RATIO OF DRAG COEFFICIENTS OF VARIOUS BODIES IN THE WAKE OF A PRIMARY BODY

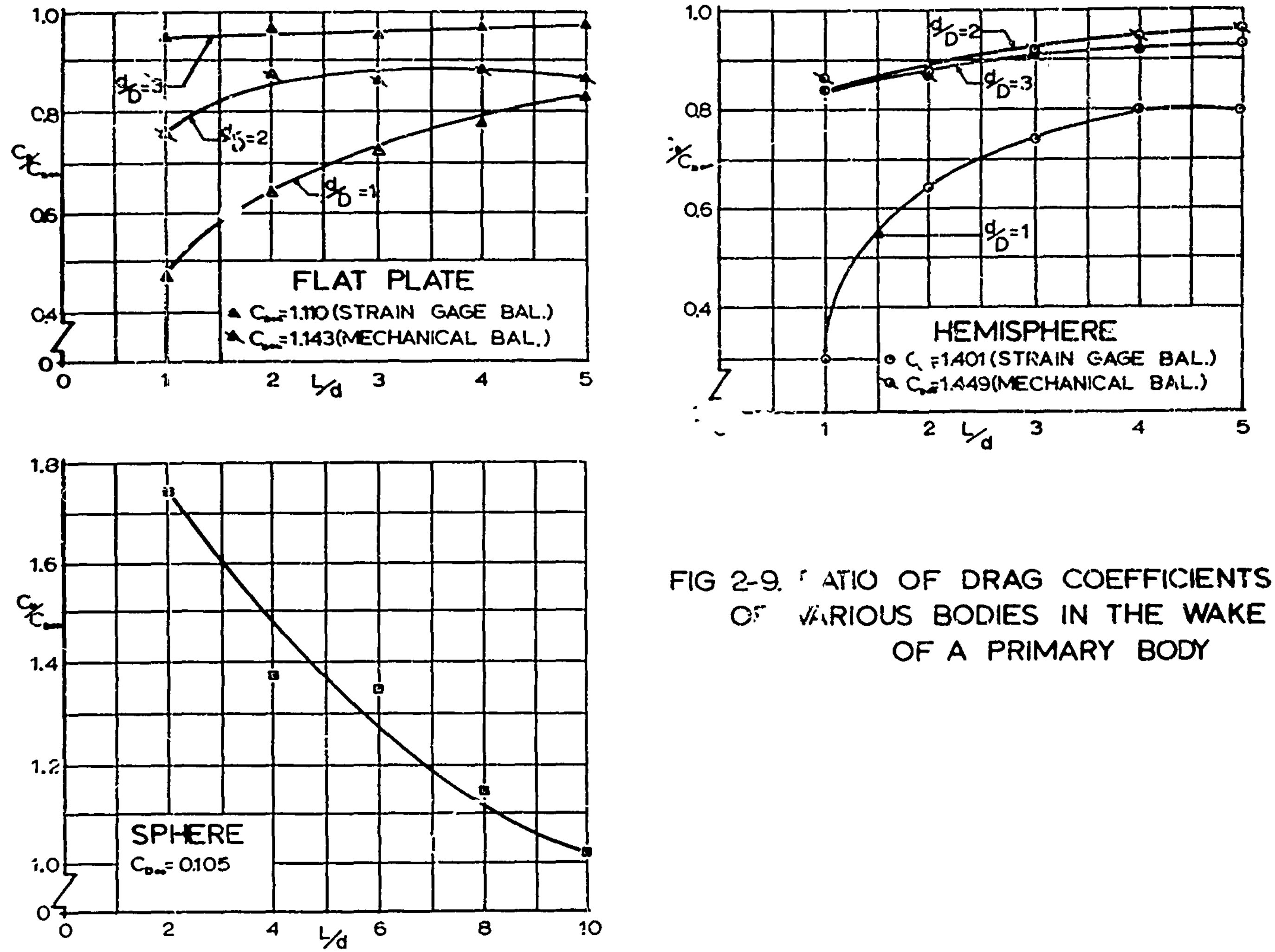

FIG 2-9. RATIO OF DRAG COEFFICIENTS OF VARIOUS BODIES IN THE WAKE OF A PRIMARY BODY

A few sample results of the wake study in compressible flow are shown in Figs 2-10 through 2-12. One recognizes all the significant phenomena of the wake effect in subsonic flow with the addition of the change in base pressure of the primary body, which leads to a noticeable variation of the drag of the system depending, among other things, on the location of the secondary body.

Studies of this nature are being continued and will be carried to higher Mach numbers (Ref 6).

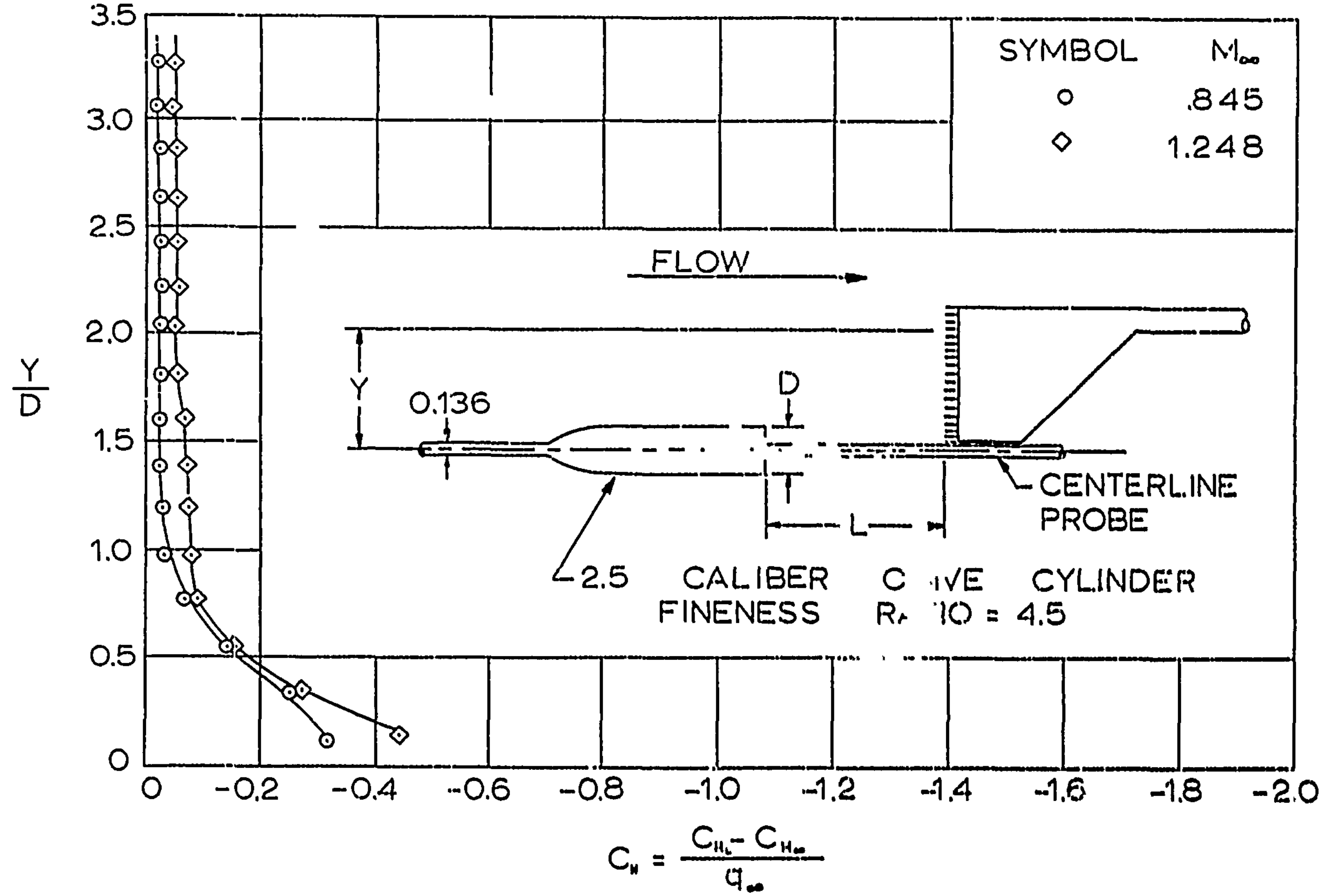

FIG 2-10. PRESSURE DISTRIBUTION IN THE WAKE OF A BODY WITH $C_{D_{INCOMP}} = 0.35$ AT A DISTANCE OF $L/D = 8.6$ IN TRANSONIC FLOW

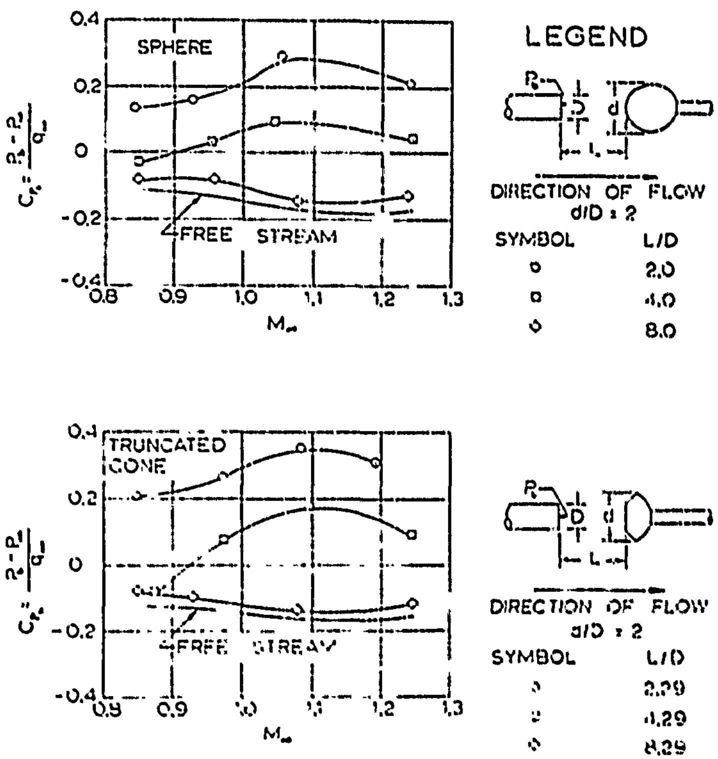

FIG. 2-11. VARIATION OF BASE PRESSURE OF THE PRIMARY BODY DUE TO THE PRESENCE OF THE SECONDARY BODY

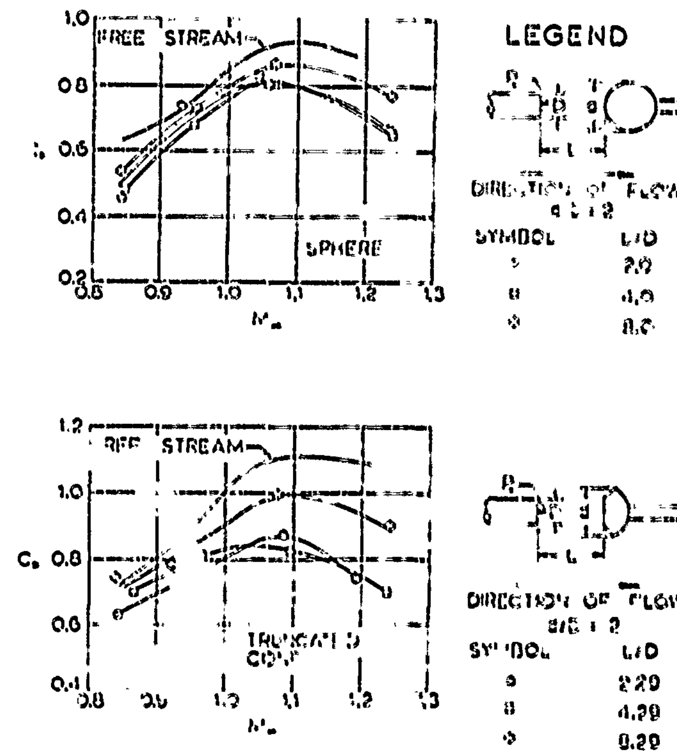

FIG 2-12. DRAG COEFFICIENT OF BODIES IN THE WAKE OF A PRIMARY BODY ($C_{D} = 0.35$) IN TRANSONIC FLOW

SECTION 3

AERODYNAMIC CHARACTERISTICS OF CONVENTIONAL PARACHUTES

Returning for the time being to the more conventional parachutes, it appears to be important to review the basic aerodynamic characteristics of the principal types of the common parachutes.

In connection with Figs 3-1 through 3-5, the principal types of the presently known par. hutes shall be briefly described.

All solid flat par nutes with medium porosity are aerodyn ically unstable . bout the position of zero degree angle of attack. Since t.e pull of the suspended load is vertical, all these parachutes will, with respect to the vertical, either oscillate, glide, or perform a combined motion. The ringslot parachutes, with considerably higher geometric porosity, are aerodynamically more stable than any of the medium porosity solid cloth parachutes. The ribbon parachutes belong also to the family of controlled geometric porosity; however, the individual units of material and open space are smaller than those of the ringslot parachute, and ribbon parachutes are in general statically and dynamically more stable than ringslot parachutes. The formed gore parachutes attempt to influence the parachute behavior through the shape of the canopy, and are characterized by the drawn

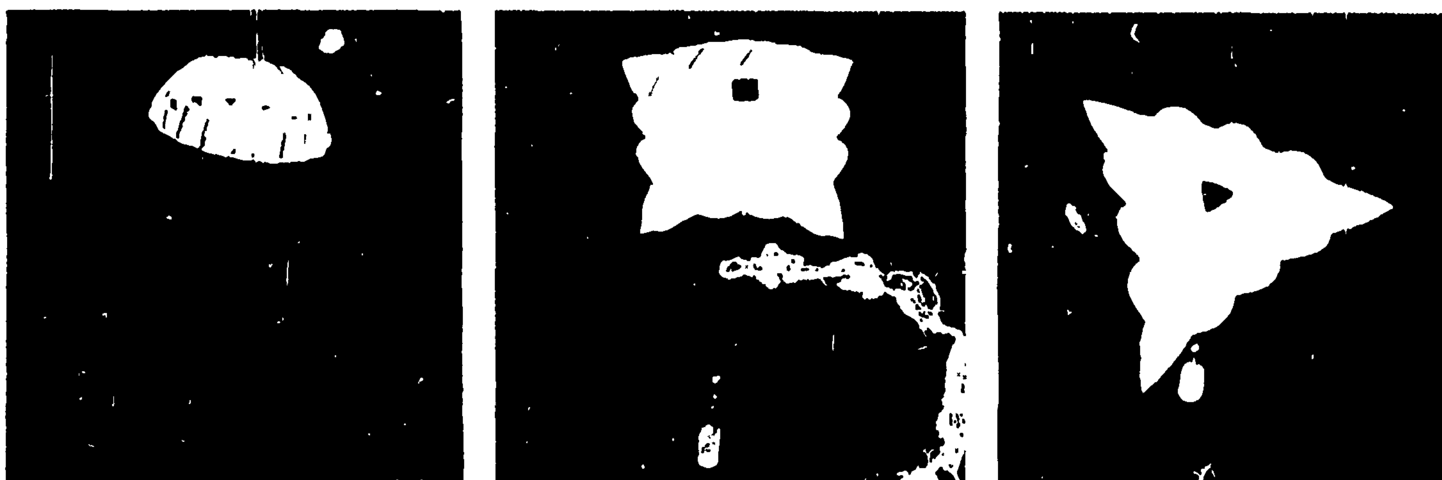

CIRCULAR SQUARE TRIANGULAR

FIG 3-1. SOLID FLAT PARACHUTES

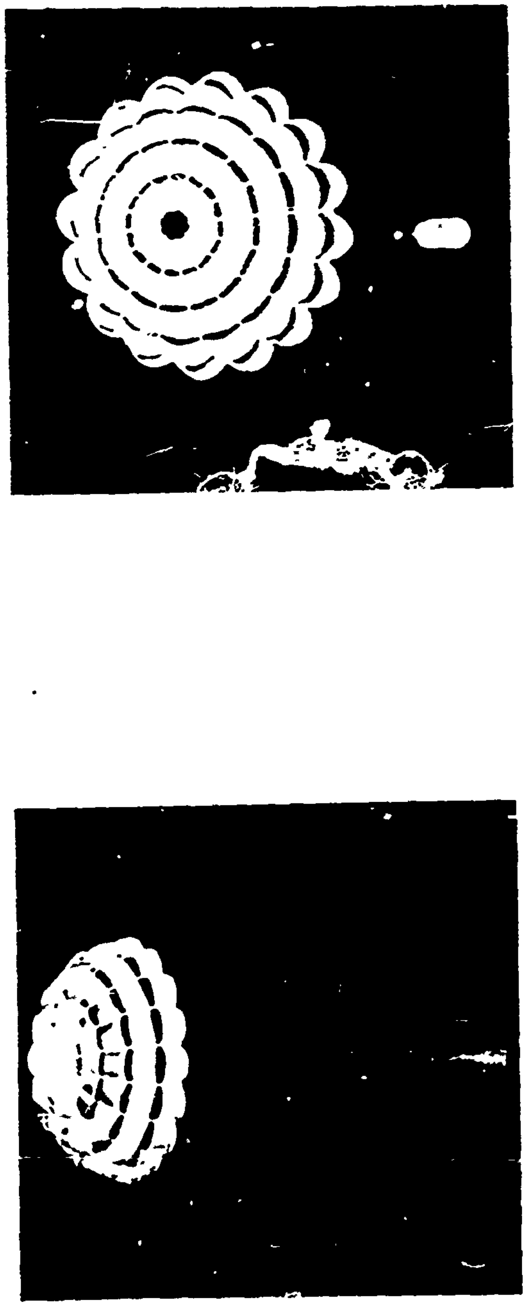

FIG 3-2. RINGSLOT PARACHUTE

CIRCULAR SQUARE TRIANGULAR

FIG 3-3. RIBBON PARACHUTES

SPHERICAL PARABOLIC EXTENDED SKIRT

FIG 3-4. FORMED GORE PARACHUTES

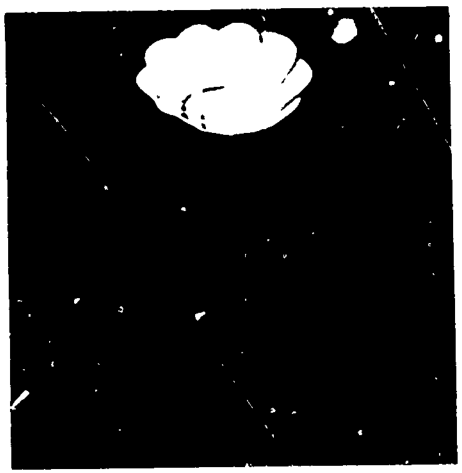

STABILIZATION

UNIVERSAL

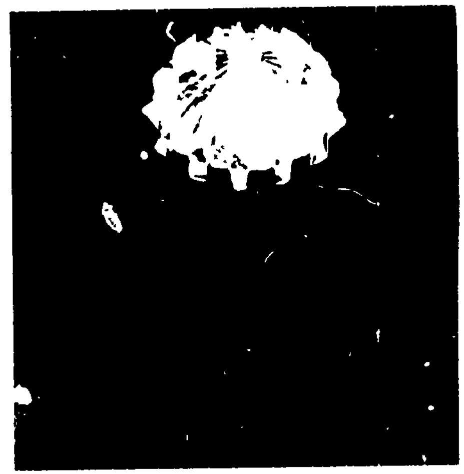

PERSONNEL

FIG 3-5. GUIDE SURFACE PARACHUTES

in skirt. These parachutes are generally more stable than the solid flat parachutes with the same cloth porosity and the same size. The most successful type in this family is the extended skirt parachute.

In the design of the guide surface parachutes, the concept of parachute shaping has been carried considerably farther. They are made of relatively low-porosity cloth, and are characterized by a pronounced conical surface at the lower portion of the canopy. The guide surface parachutes are the most stable parachutes in their respective classes. Three standard types have been developed, namely, for stabilization with a minimum amount of drag, for stabilization and retardation, and for primary retardation purposes (with a stability characteristic better than the extended skirt but not as good as the ribbon parachute).

These are only the more common types; numerous other designs have been proposed with more but minor variations. Their performance characteristics are within the limits of the discussed types. Rotating parachutes represent an entirely new group and may gain significance. However, it is too early to make definite statements.

The stability behavior of a parachute depends primarily on its static stability. If the angle of attack is measured between the longitudinal axis of the parachute and the direction of the undisturbed flow, and stability is defined by an aerodynamic moment opposing the deflection from the zero position ($C_M > 0$ for $\alpha > 0$) and a positive $dC_M/d\alpha$, the stability characteristics of a number of parachutes can be recognized from Figs 3-6 through 3-8.

These figures show a number of facts which indicate the significance of the porosity of the canopy material upon the aerodynamic stability of the parachute.

Figure 3-6 shows that the rigid but slotted hemisphere, an idealized Ribbon parachute, is unstable at its zero position even when the open areas amount to 35% of the entire surface. The flexibility of textile material and the deviation from the hemispherical form is needed to make a real ribbon parachute stable.

Figure 3-7 shows that hollow truncated cone, represented by a guide surface parachute, is statically stable and depends only lightly on porosity.

Figure 3-8 shows that solid cloth parachutes, which are unstable when built out of non-porous flexible material, do become stable if a high degree of porosity is allowed. However, one has to consider that parachutes with a very high porosity may fail to inflate, which generally impairs their usefulness.

Figures 3-9 and 3-10 show, for the same parachutes, the normal and tangential force coefficients and their dependency on the cloth porosity.

A further analysis of these results appears to be interesting and desirable.

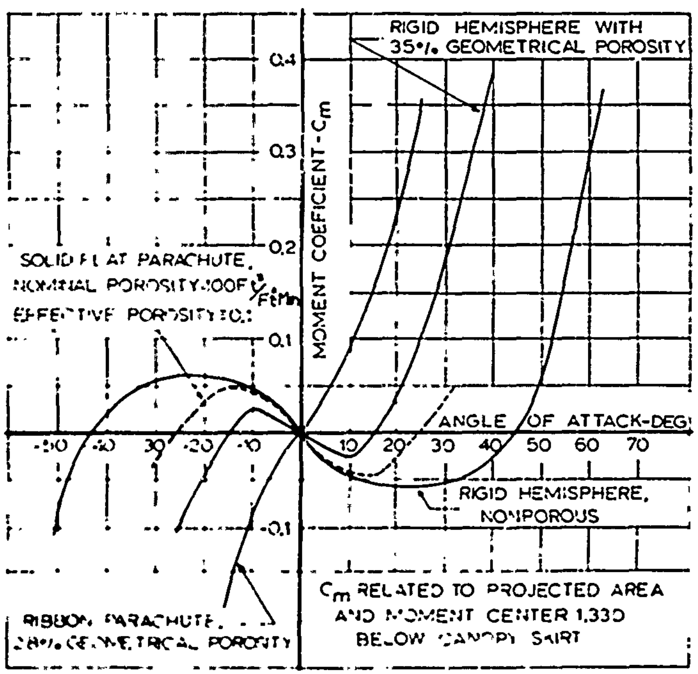

FIG 3-6. MOMENT COEFFICIENT VERSUS ANGLE OF ATTACK OF RIBBON PARACHUTES AND POROUS AND NONPOROUS HEMISPHERES

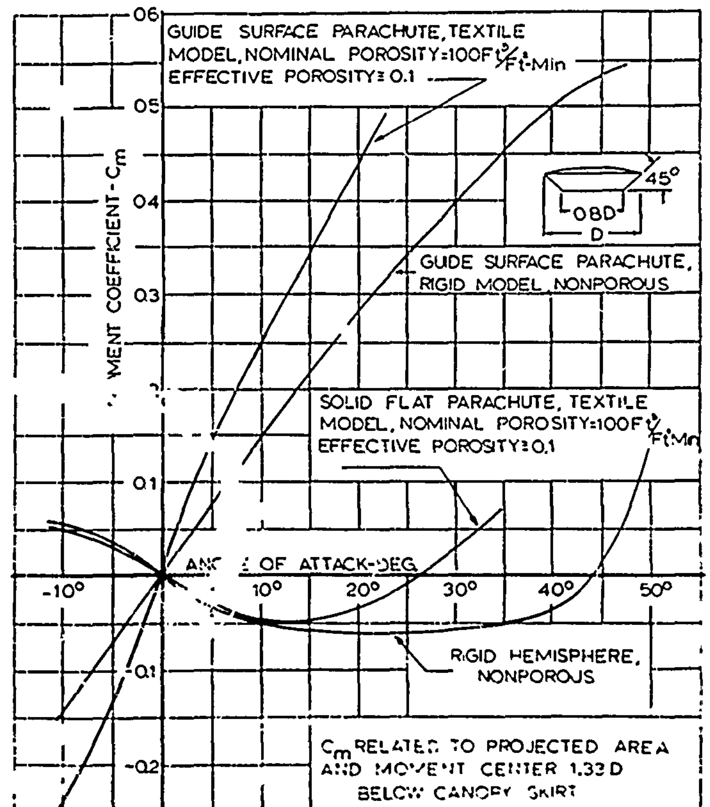

FIG 3-7 MOMENT COEFFICIENT VERSUS ANGLE OF ATTACK OF GUIDE SURFACE PARACHUTES AND POROUS AND NONPOROUS HEMISPHERES

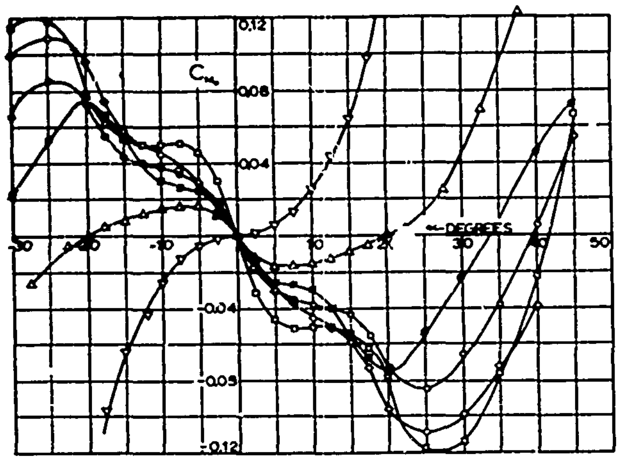

CIRCULAR FLAT

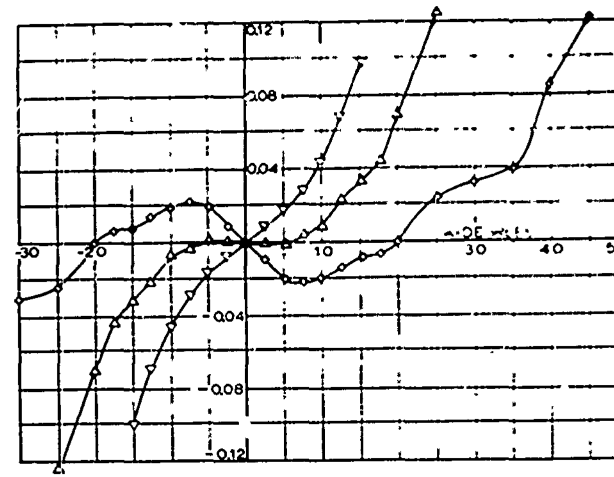

PERSONNEL GUIDE SURFACE

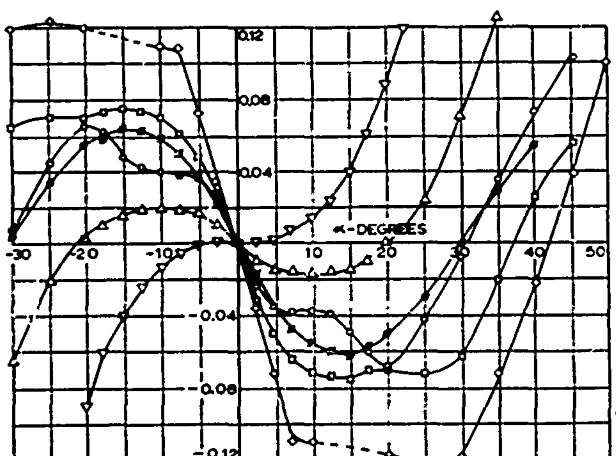

10% EXTENDED SKIRT

SYMBOL	NOMINAL POROSITY (FT³/FT²-MIN)	EFFECTIVE POROSITY
▽	[illegible]	0.096
△	20	0.042
●	30	0.010
○	10	0.003
◇	0	0.0 (RIGID)
□	0	0.0 (POLY)

FIG. 3-8. MOMENT COEFFICIENT VERSUS ANGLE OF ATTACK OF VARIOUS PARACHUTES

BASED ON TOTAL CLOTH AREA

REYNOLDS NO. ≈ 6×10^5

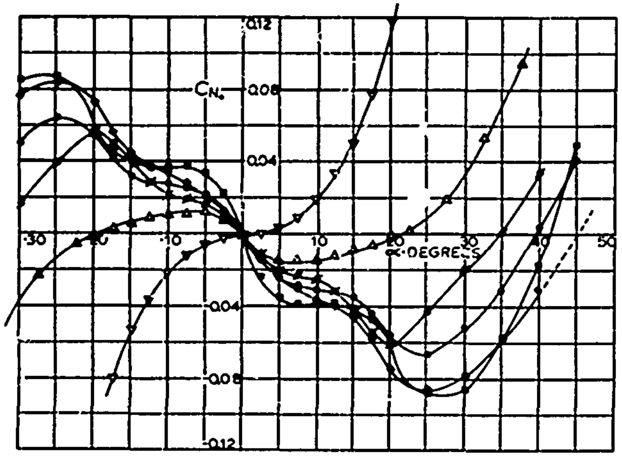

CIRCULAR FLAT

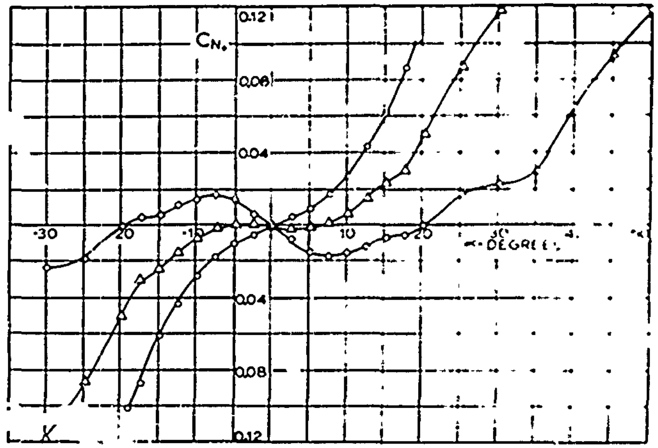

PERSONNEL GUIDE SURFACE

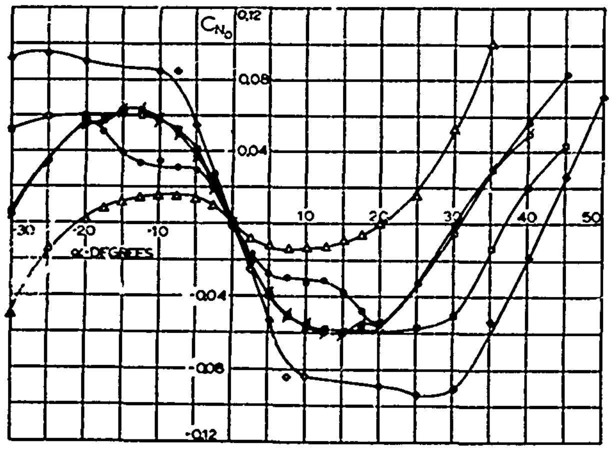

10% EXTENDED SKIRT

SYMBOL	NOMINAL POROSITY (FT³/FT²-MIN)	EFFECTIVE POROSITY
▽	5	0.096
△	10	0.042
■	10	0.010
○	10	0.003
◇	0	0.0 (RIGID)
□	0	0.0 (POLY)

FIG. 3-9. NORMAL FORCE COEFFICIENT VERSUS ANGLE OF ATTACK OF VARIOUS PARACHUTES

BASED ON TOTAL CLOTH AREA

REYNOLDS NO. = 6×10^5

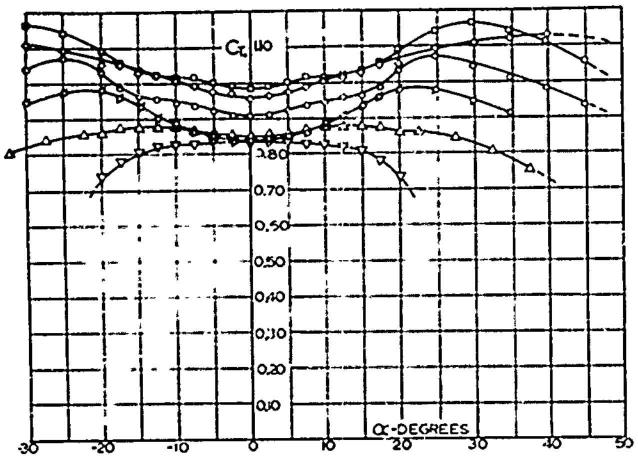

CIRCULAR FLAT

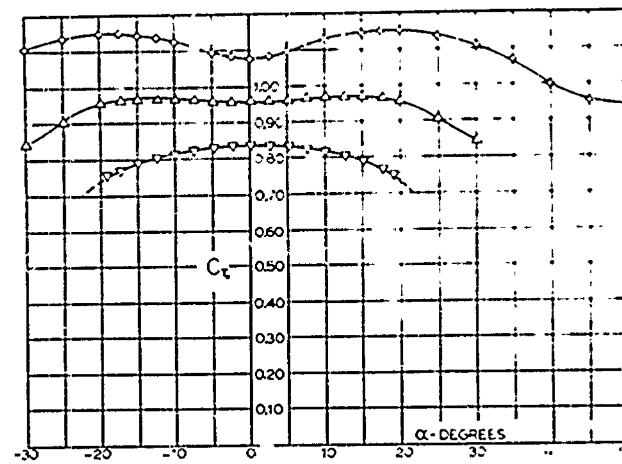

PERSONNEL GUIDE SURFACE

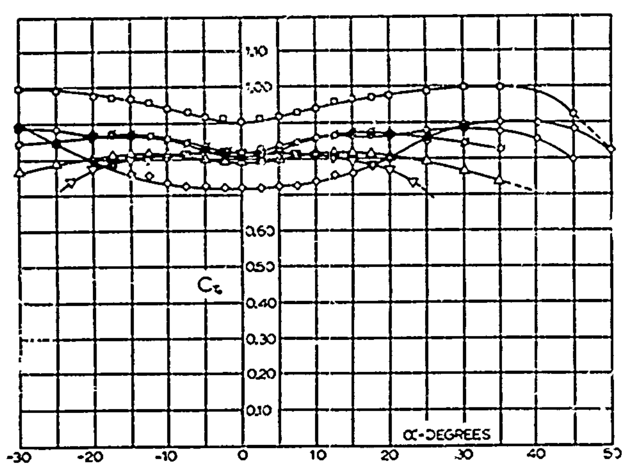

10% EXTENDED SKIRT

SYMBOL	NOMINAL POROSITY (FT^3/FT^2-MIN)	EFFECTIVE POROSITY
▽	75	0.096
△		0.042
●	30	0.010
○	0	0.003
◇	0	0.0 (R-D)
□	0	0.0 (POLY)

FIG 3-10. TANGENT FORCE COEFFICIENT VERSUS ANGLE OF ATTACK OF VARIOUS PARACHUTES

BASED ON TOTAL CLOTH AREA

REYNOLDS NO. ≃ 6×10^5

The next large problem area of parachutes is the time of inflation and the opening force, and Figs 3-11 through 3-13 illustrate the characteristic features of opening time and opening force versus velocity and altitude. It may be surprising that for constant indicated air speed, all known solid cloth parachutes show a remarkable increase of opening force with increasing altitude. In a descriptive manner this phenomenon may be understood if one considers the process of inflation of a parachute as a change of momentum, and the time duration of this process follows from the mass balance between the entering air and the air lost through the porous material of the parachute canopy. If now the ratio between the escaping and entering air, so to speak, the effective porosity of the material, decreases with altitude, which physically means with decreasing air density, the faster inflation and higher average opening force can be understood. A quantitative treatment of this process will be given later. For the time being a statement may be accepted that the porosity of the material and its change with density, which represents merely a dependency of the screen drag of the material with Reynolds number, primarily cause the increase of opening force with altitude (Refs 7 and 8).

In summary, the porosity of the parachute material influences strongly not only the static stability, side force, and drag, but also the dynamics of the opening

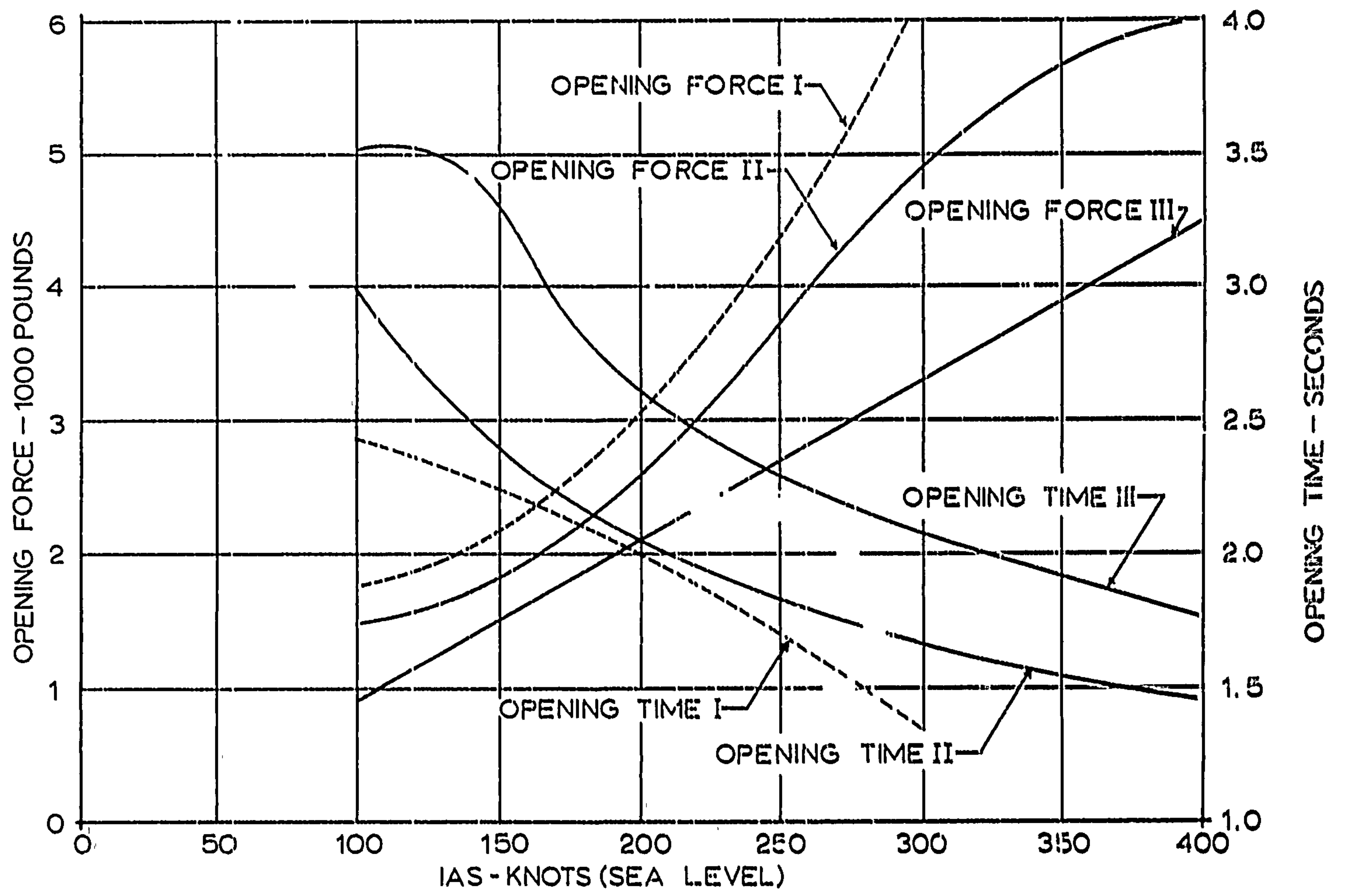

FIG 3-11. OPENING FORCE AND OPENING TIME OF (I) CIRCULAR FLAT PARACHUTE, (II) CIRCULAR FLAT PARACHUTE IN QUARTER BAG, AND (III) PERSONNEL GUIDE SURFACE PARACHUTE VS SPEED AT SEA LEVEL DENSITY. (ALL PARACHUTES HAVE A DRAG AREA OF 490 FT^2 AND A CANOPY LOADING OF 0.323 lb/ft^2) COURTESY OF U.S.A.F

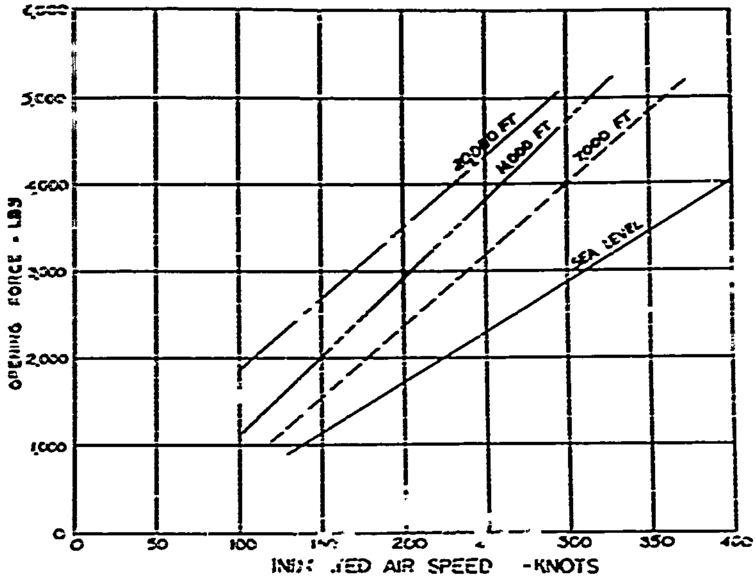

FIG 3-12. OPENING FORCE OF THE PERSONNEL GUIDE SURFACE PARACHUTE VERSUS SPEED AT VARIOUS ALTITUDES COURTESY U.S.A.F.

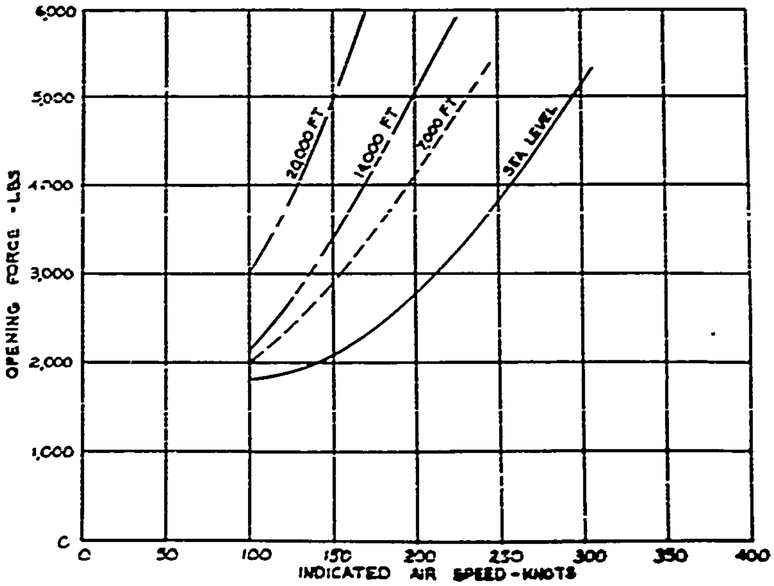

FIG 3-13. OPENING FORCE OF THE CIRCULAR FLAT PARACHUTE VERSUS SPEED AT VARIOUS ALTITUDES

COURTESY U.S.A.F.

parachute, and a detailed investigation of the porosity characteristics of textile materials appears to be highly desirable.

SECTION 4

THE EFFECTIVE POROSITY

4.0 Introduction

As discussed in the preceding section, it is known that the opening shock of solid cloth parachutes increases with altitude; also, the oscillations of basically unstable parachutes become more violent (Refs 9 and 10).

Attempts have been made to explain the change of the inflation characteristics through the effect of the apparent mass and the mass of air included in the parachute canopy (Ref 11). The variation of the stability behavior of a parachute may in part also be attributed to the effect of apparent and included mass, because the motion of a freely descending parachute is a matter of dynamic stability in which the related air masses are significant terms.

However, it is also known that the stability behavior of a parachute depends on the porosity of its canopy (Refs 12 and 13). In combination with experience at higher altitudes, this leads to the conclusion that the porosity or air permeability of woven sheets is effectively being reduced at higher altitudes. If this assumption is correct, it would also, at least in part, account for the increase of opening shock with altitude.

These aspects are discussed in Ref 14, where it was also shown that the apparent mass of a parachute varies with the porosity of the canopy. In view of this interaction of performance characteristics and porosity, studies were made in which the air flow through woven porous sheets was measured, and correlated with air density and pressure. The results of these efforts will be presented in the following sections of this report.

4.1 List of Symbols

U	=	Average velocity of flow through porous surface
V	=	Free stream velocity
ρ	=	Density
ρ_0	=	Density at sea level
σ	=	Density ratio
μ	=	Viscosity
μ_o	=	Viscosity at sea level
$C = U/V$	=	Effective porosity
C_o	=	Effective porosity at sea level
Q	=	Flow rate
Δp	=	Pressure differential across porous material
Δp_{crit}	=	Pressure differential across porous material necessary for sonic velocity in the openings
n	=	Exponent as defined in equation (4.10).

4.2 Definition of the Effective Porosity

The porosity, also called air permeability, is conventionally expressed as the volumetric flow rate of air per unit of cloth area under a certain differential pressure. Figure 4-1 shows a typical diagram of this nominal porosity versus differential pressure for three commonly used parachute materials.

For performance calculations, a dimensionless term is preferable which, for example, would relate the average velocity, U, through the porous surface to the dynamic pressure of a fictitious velocity, V. Figure 4-2 shows schematically the cloth as a grid in free air flow. The velocity in the free stream shall be V, and its related dynamic pressure, $(\rho/2)\,V^2$, shall be assumed to be identical to the differential pressure, Δp, across the cloth. The ratio U/V shall be called the "effective porosity." Figure 4-3 shows the effective porosity of the previously mentioned parachute materials.

Considering the cloth as a porous screen leads to the idea of treating the flow through the cloth as a function

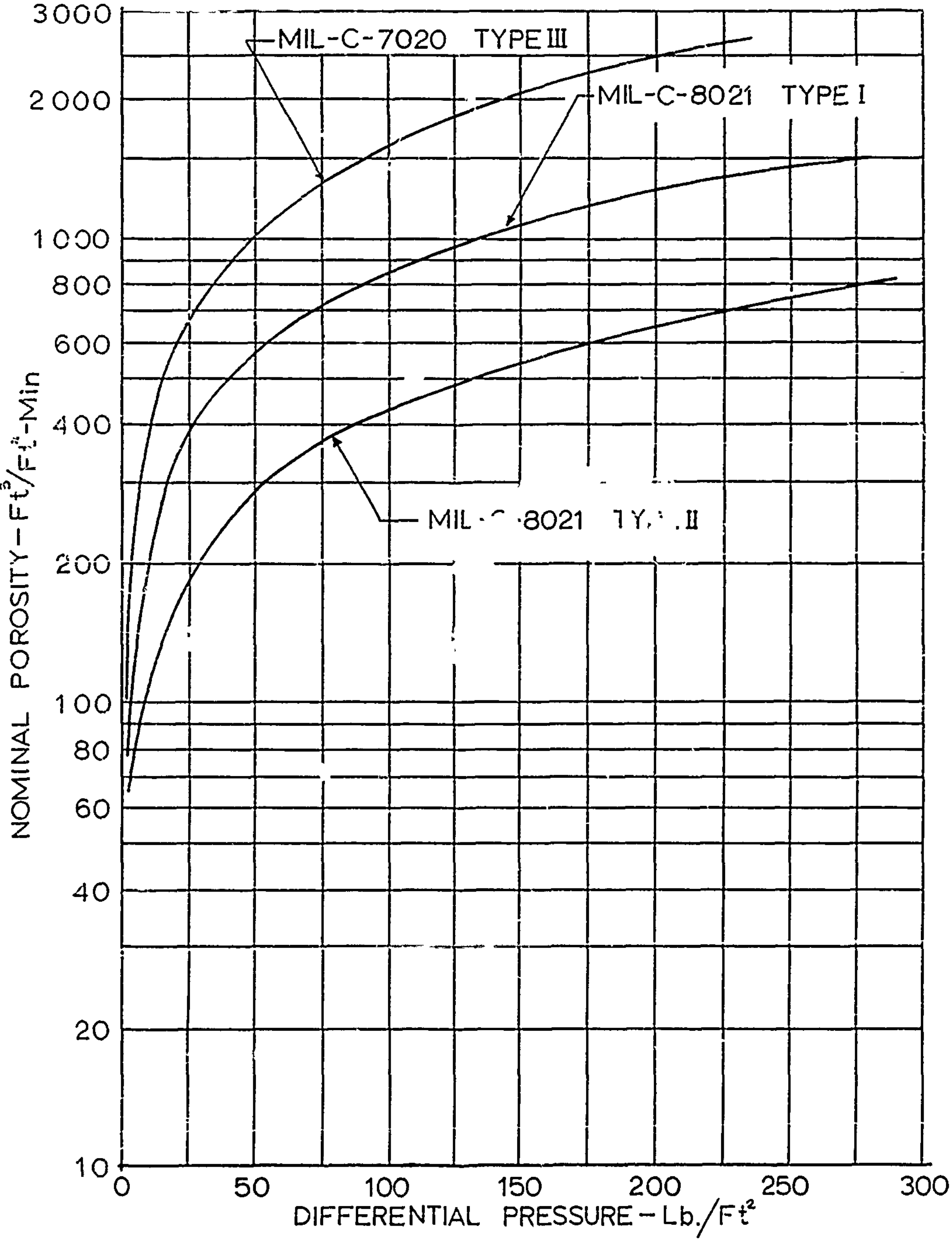

FIG 4-1. NOMINAL POROSITY OF PARACHUTE MATERIALS VERSUS DIFFERENTIAL PRESSURE

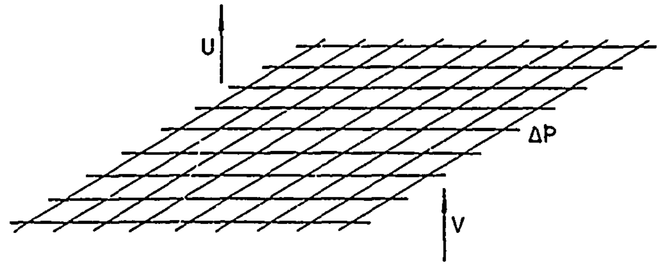

EFFECTIVE POROSITY $C = \frac{U}{V}$

WITH $\Delta P = \frac{\rho}{2} V$, $C = \frac{U}{\sqrt{\frac{2 \Delta p}{\rho}}}$

FIG 4-2. DERIVATION OF THE TERM "EFFECTIVE POROSITY"

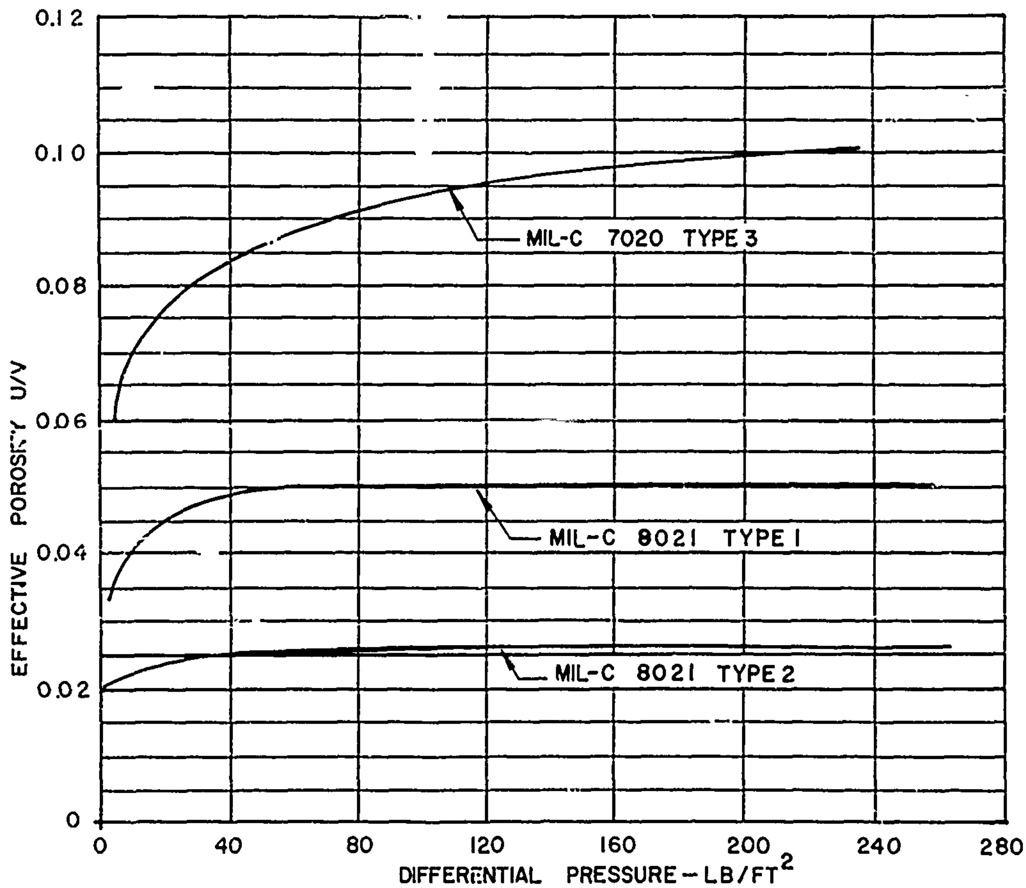

FIG 4-3. THE EFFECTIVE POROSITY OF PARACHUTE MATERIALS VERSUS DIFFERENTIAL PRESSURE.

of the ratio of the open to the solid area and as a consequence of the air resistance of the individual threads. If one further assumes that the threads or yarns are circular cylinders, one may attempt to compute the air resistance of the woven sheet from the viscous drag of the individual cylinders. A number of investigations have been carried out in this manner (Refs 15, 16, and 17). However, the microscopic photographs of the four sample materials shown in Fig 4-4 indicate that the assumption of a simple geometry for the cloth may be an oversimplification, and a purely analytical treatment of the drag problem could not encompass a number of eventually very significant characteristics. Therefore, the actual mass flow through the cloth has been measured.

Figures 4-1 and 4-3 indicate that the mass flow through the cloth increases with the differential pressure. One may assume that this relationship will exist in a monotonic manner until the critical pressure differential is reached at which the velocity through the orifices reaches the speed of sound. A further increase of the differential

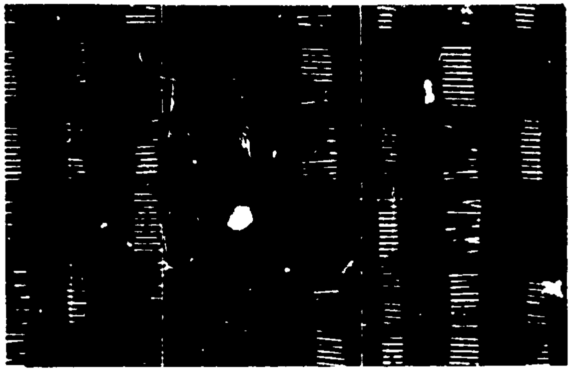

MIL-C-7020 TYPE I, 40$\frac{lb}{in}$ NYLON, t=0.0032"

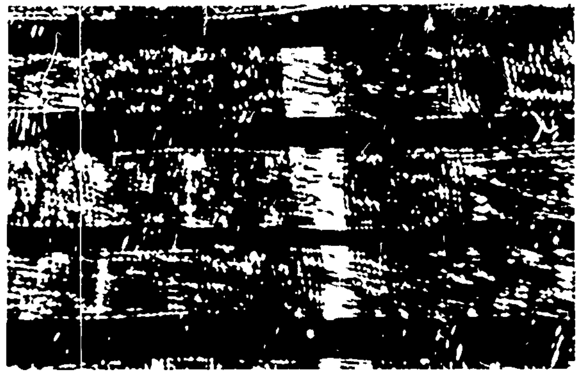

MIL-C-7350 TYPE 1 100$\frac{lb}{in}$ NYLON, t=0.006"

0 0.05"

MIL-C-8020 TYPE I, 200$\frac{lb}{in}$ NYLON, t=0.020"

MIL-C-8020 TYPE II, 300$\frac{lb}{in}$ NYLON, t=0.024"

FIG 4-4. MICROSCOPIC PHOTOS OF FOUR GENERALLY USED PARACHUTE MATERIALS pressure will then not further increase the air velocity. Therefore, it appears to be advisable to study the flow with respect to the incompressible and compressible flow regimes.

If one first considers incompressible flow, one may assume that the air flows through the fine orifices of a relatively thick cloth somewhat like through a pipe in which the motion is neither completely laminar nor fully turbulent. Therefore, an analysis of the two border cases seems to be in order.

For fully developed laminar flow, Hagen-Poiseuille's law with the following relationship would be applicable:

$$\Delta p = \frac{128 \mu L Q}{\pi D^4} , \tag{4.1}$$

in which L = Length of the tube

D = Diameter of the tube.

With $Q = U \pi D^2/4$, the average velocity in the pipe may be written

$$U = \frac{D^2}{32 \mu L} \Delta p . \tag{4.2}$$

If the Hagen-Poiseuille relationship is applicable, one may present the effective porosity as

$$C = \frac{U}{V} = \frac{D^2}{32 \mu L} \sqrt{\frac{\rho \Delta p}{2}} \tag{4.3}$$

and specifically for sea level density

$$C_o = \left(\frac{U}{V}\right)_o = \frac{D^2}{32\mu_o L}\sqrt{\frac{\rho_o \Delta p}{2}} \quad . \tag{4.3a}$$

For the first approximation one may set $\mu = \mu_o$. Then the effective porosity for any altitude with $\rho/\rho_o = \sigma$ and for the same differential pressure may be written

$$C = C_o \, \sigma^{\frac{1}{2}} . \tag{4.4}$$

A similar analysis may be made for the assumption of fully developed turbulent flow. With the Blasius formula (Ref 1)

$$\frac{\Delta p}{L} = \frac{\lambda}{D} \, \frac{\rho}{2} \, U \tag{4.5}$$

and

$$\lambda = 0.3164 \left(\frac{U \rho D}{\mu}\right)^{-\frac{1}{4}} \tag{4.6}$$

the velocity follows as

$$U = \left(\frac{2 \Delta p D^{5/4}}{0.3164 \, L}\right)^{\frac{4}{7}} (\mu \rho^3)^{-\frac{1}{7}} . \tag{4.7}$$

Using $V = (2\,\Delta p/\rho)^{\frac{1}{2}}$ and the subscript zero for sea level density, the effective porosity C may be written

$$\frac{C}{C_o} = \left(\frac{\Delta p}{\Delta p_o}\right)^{\frac{1}{14}} \left(\frac{\mu_o}{\mu}\right)^{\frac{1}{7}} \left(\frac{\rho}{\rho_o}\right)^{\frac{1}{14}} . \tag{4.8}$$

With $\mu = \mu_o$, and for the same differential pressure, one obtains for fully developed turbulent flow

$$C = C_o \, \sigma^{\frac{1}{14}} . \tag{4.9}$$

The assumption of both laminar and turbulent flow in the region of incompressibility leads to a relationship of the form

$$C = C_o \sigma^n , \tag{4.10}$$

and it is now the objective of experiments to establish the value of the exponent "n" for various types of parachute material.

When the differential pressure, Δp, reaches or exceeds the critical value, one may assume that sonic flow through the orifices is established; any additional pressure will not cause a further increase of the flow velocity, and beginning at this point the effective porosity will decline when the pressure increases. These conditions will occur in all transonic and supersonic parachute operations. Therefore it appears to be advisable to introduce, besides the density ratio σ , the pressure ratio $\Delta p/\Delta p_{crit}$ as a significant parameter.

Disregarding secondary effects such as discharge coefficients, geometric porosity, etc., one may expect that also in the regime of compressible flow the effective porosity may be conveniently expressed in the form $C = C_o \sigma^n$. However, the numerical value of the exponent "n" will probably differ from the one found for the incompressible flow regime.

4.3 Measurements of the Effective Porosity

In view of the analysis above, the effective porosity of four standard textile materials was measured by means of the apparatus shown in Fig 4-5. Figures 4-6 through 4-13 show their effective porosity, C, as a function of the density ratio, σ ; and the pressure ratio, $\Delta p/\Delta p_{crit}$, respectively. It may be pointed out that the density ratio is related to the free stream conditions downstream of the porous screen. Figures 4-14 and 4-15 are si[illegible] [illegible]cordings for a wire screen with a nominal po[illegible]ity in th[illegible] order of the cloth porosities. The wire s[illegible]een has been incorporated in the study [illegible]ecause the texti[illegible] screens may change their geometry under the pressure load[illegible]ng and therefore their porosity reflects not only Reynolds and Mach number effects but also unknown consequences of the elasticity of the cloth.

As can be seen, the wire screen shows the same characteristics as the more elastic textile screens, and it appears to be justified to assume that for the investigated parachute materials the elasticity is of secondary significance.

For the analysis of the phenomenon which actually takea place, it may be said that the Figs 4-6 through 4-13 reflect the influence of Reynolds as well as Mach number. For example, it can be seen that the effective porosity versus σ for pressure differentials $\Delta p/\Delta p_{crit}$ between 0.1 and

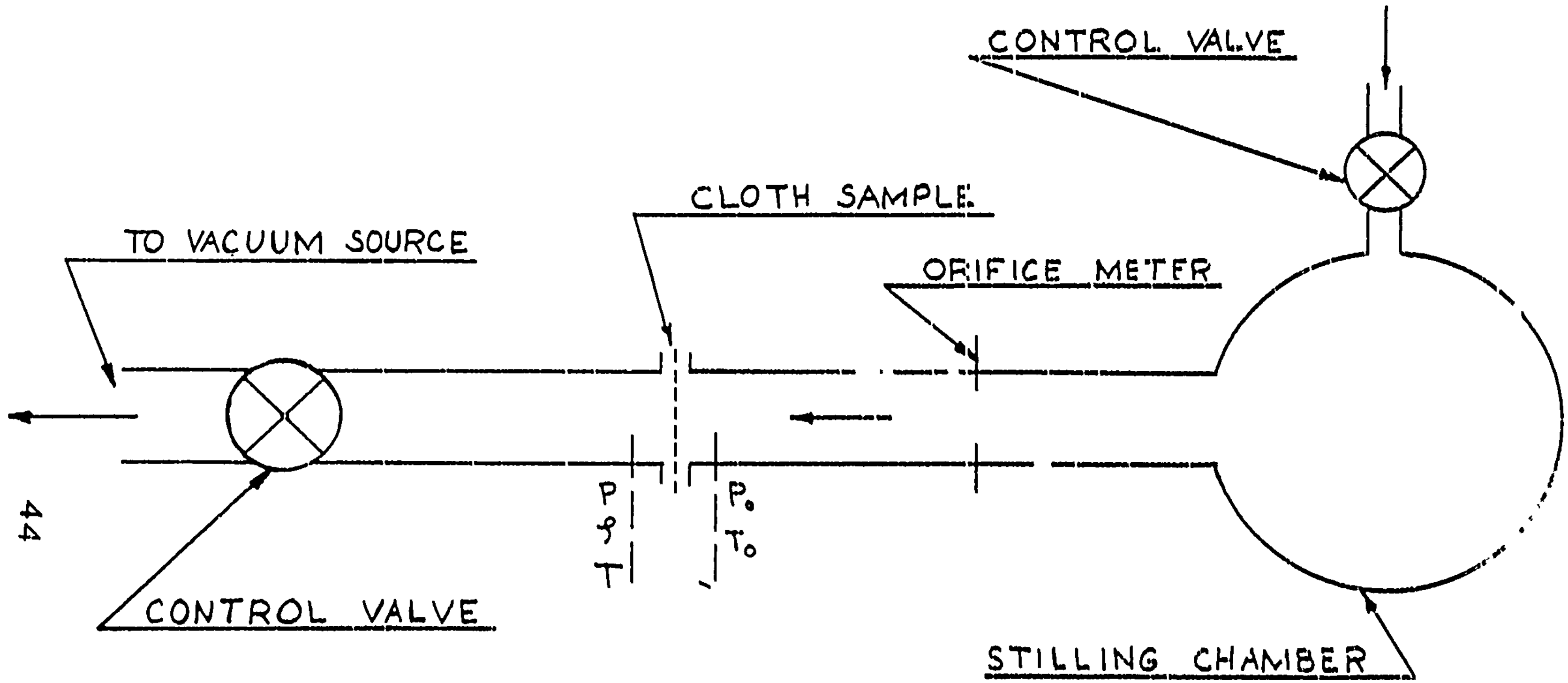

FIG 4-5. POROSITY MEASURING APPARATUS

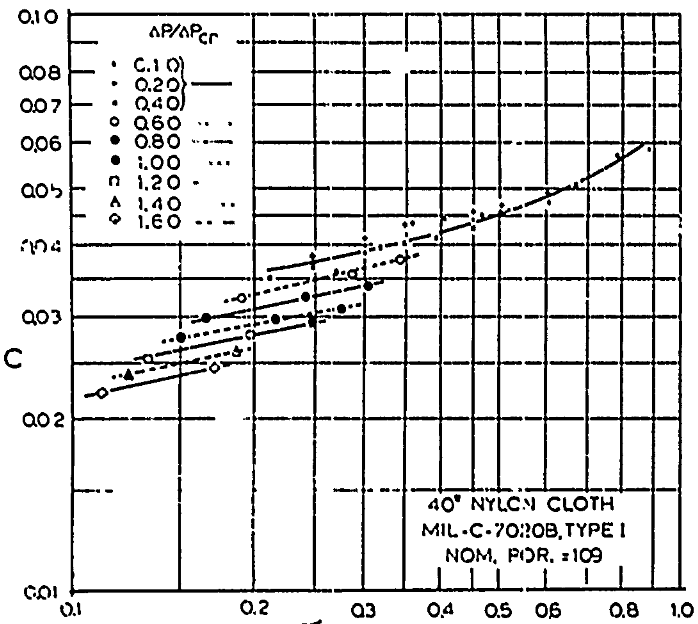

FIG 4-6. EFFECTIVE POROSITY VERSUS DENSITY RATIO

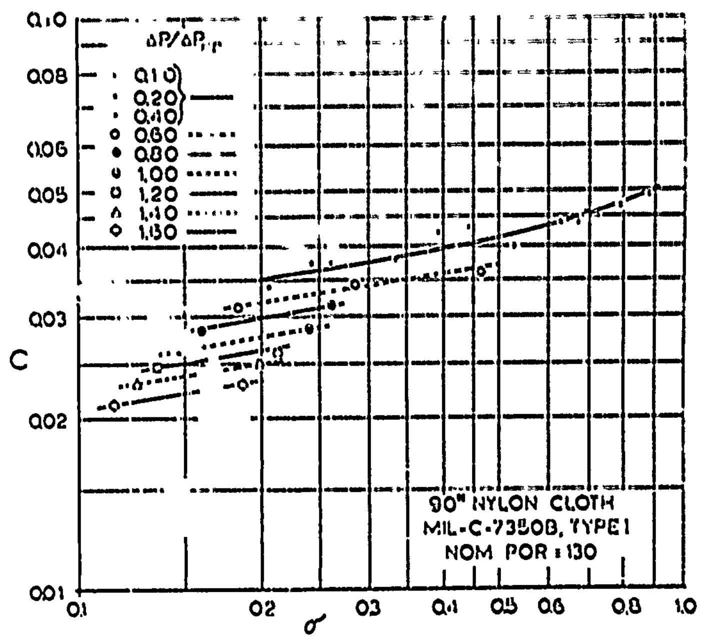

FIG 4-7. EFFECTIVE POROSITY VERSUS DENSITY RATIO

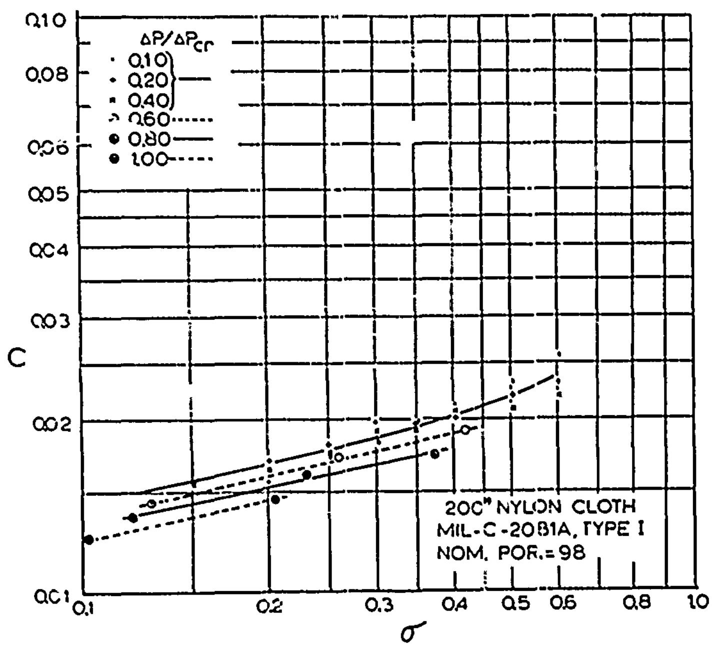

FIG 4-8. EFFECTIVE POROSITY .VERSUS DENSITY RATIO

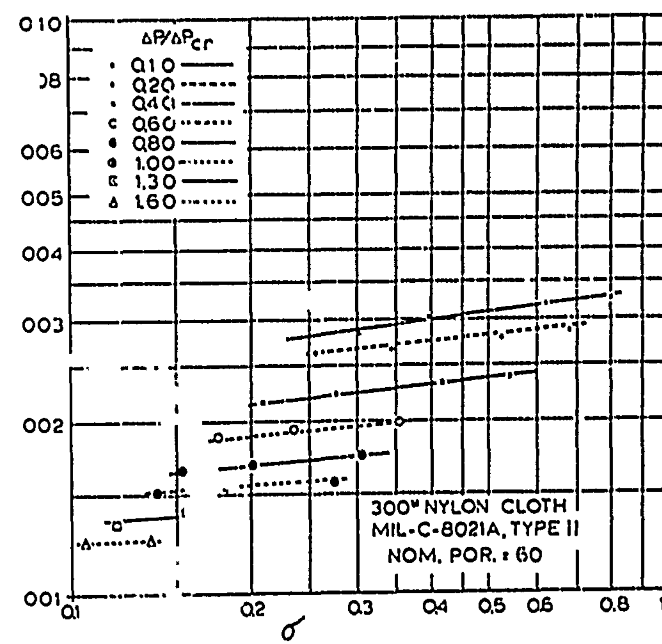

FIG 4-9. EFFECTIVE POROSITY VERSUS DENSITY RATIO

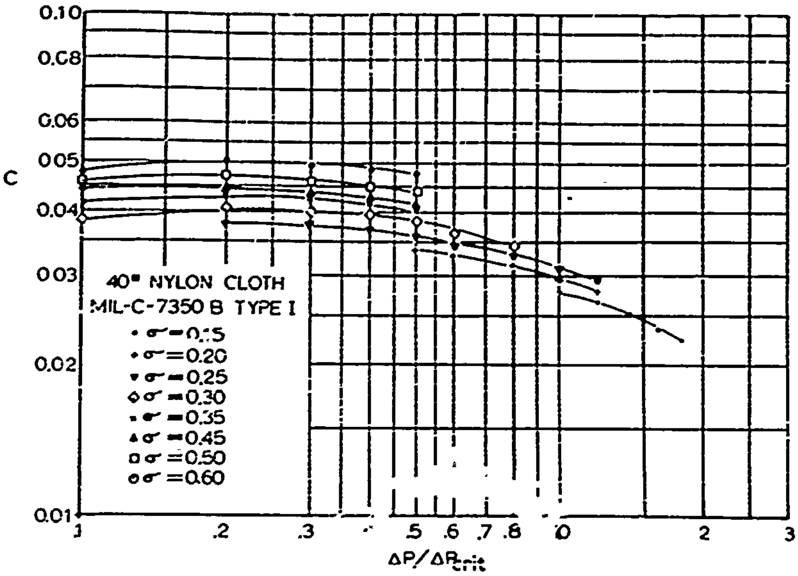

FIG 4-10. EFFECTIVE POROSITY VERSUS PRESSURE RATIO

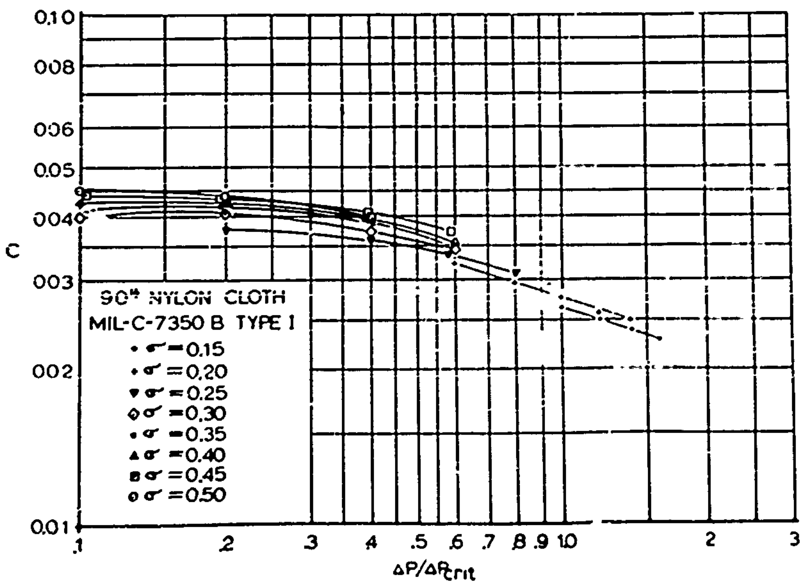

FIG 4-11. EFFECTIVE POROSITY VERSUS PRESSURE RATIO

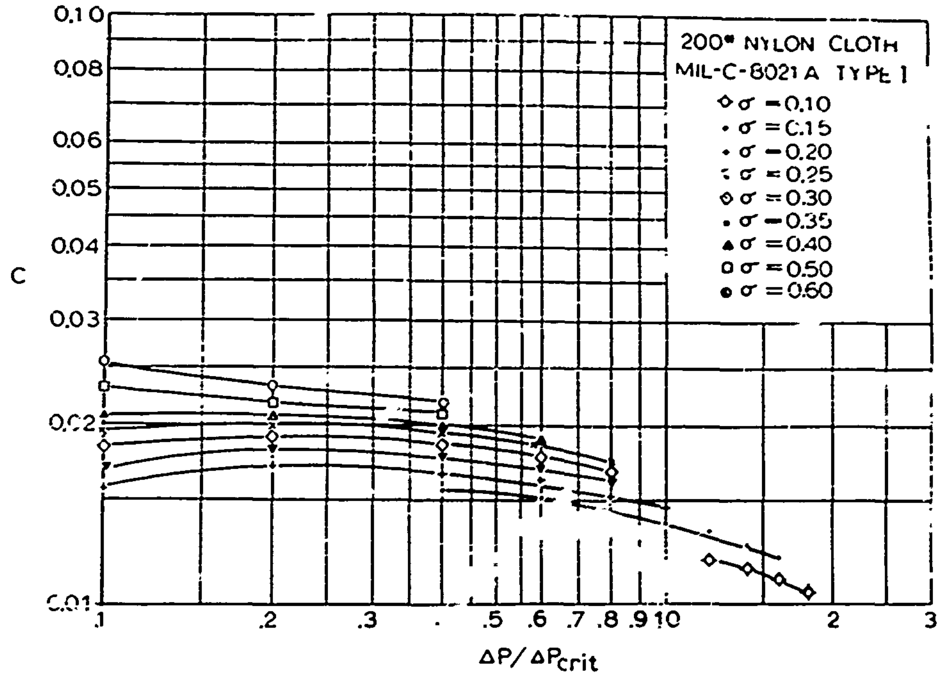

FIG 4-12 EFFECTIVE POROSITY VERSUS PRESSURE RATIO

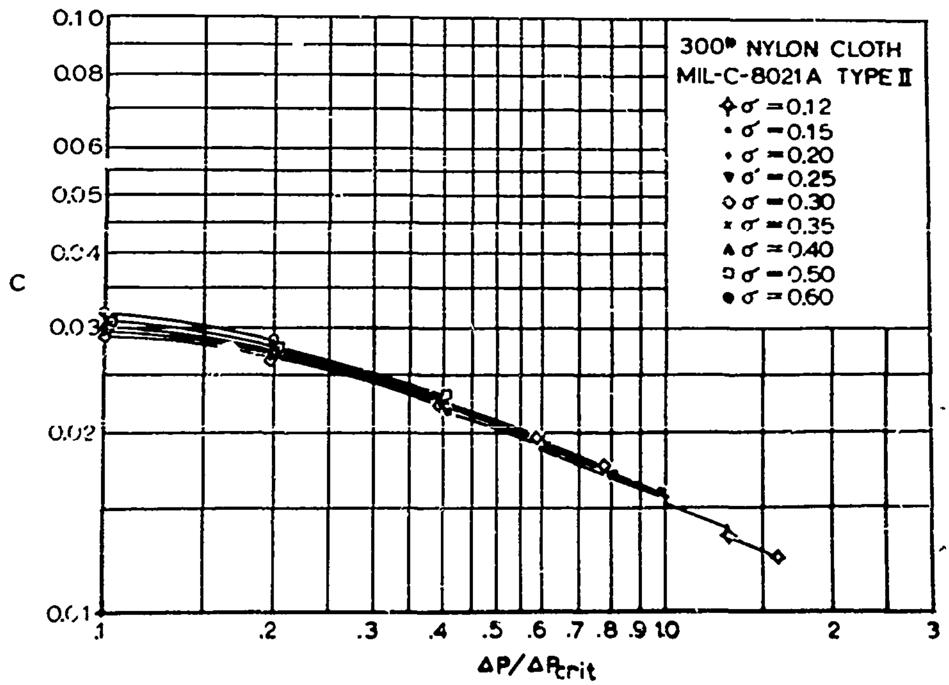

FIG 4-13. EFFECTIVE POROSITY VERSUS PRESSURE RATIO

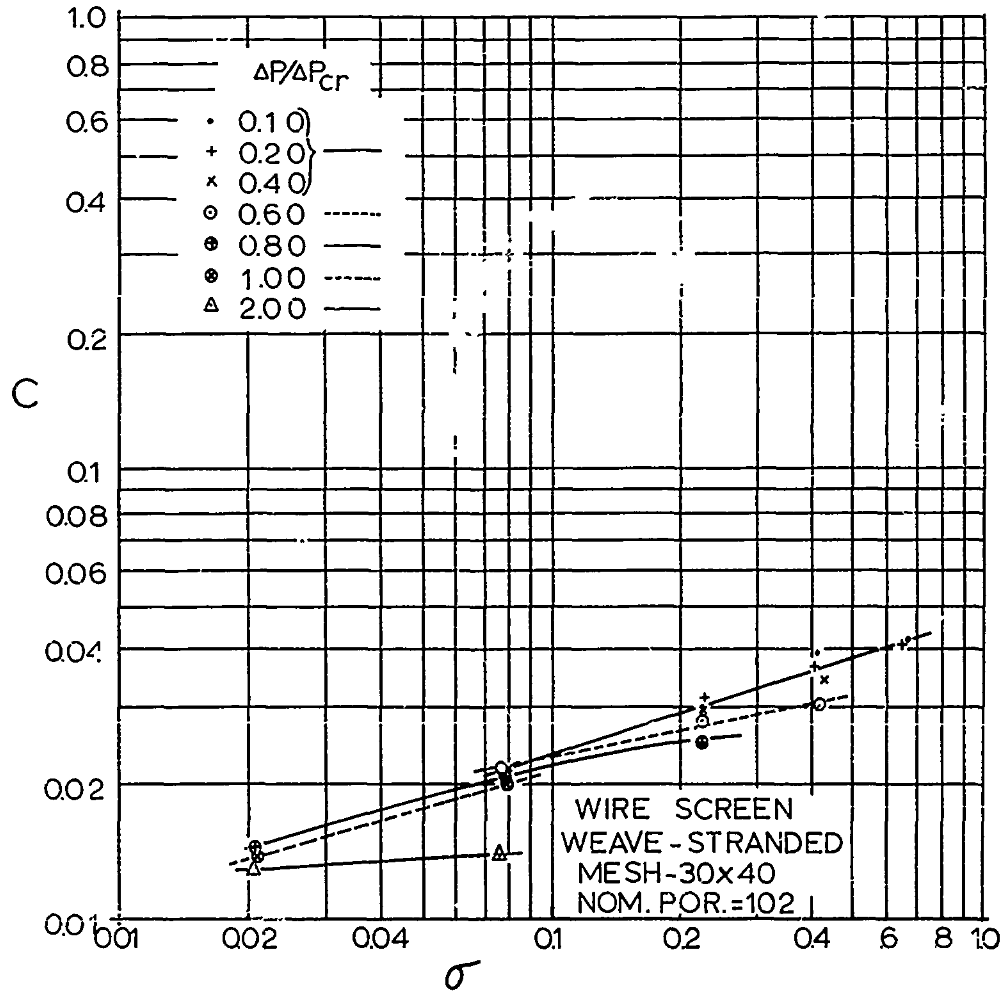

FIG 4-14. EFFECTIVE POROSITY VERSUS DENSITY RATIO

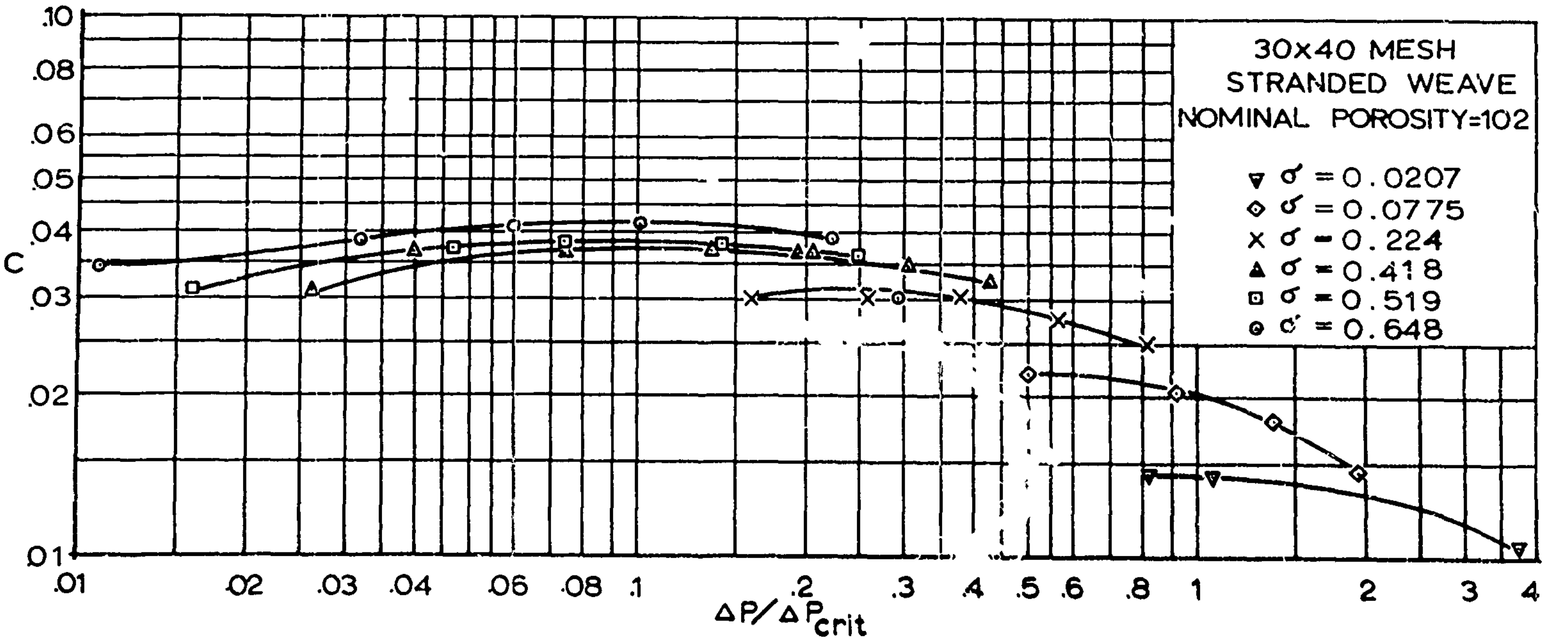

FIG 4-15. EFFECTIVE POROSITY OF A WIRE SCREEN VERSUS PRESSURE RATIO

0.4 is essentially the same. These curves are related to the incompressible flow regime and the variation of the effective porosity is primarily a Reynolds number effect. In the region of higher pressure differentials, in which $\Delta p/\Delta p_{crit}$ approaches or exceeds unity, a certain change in the absolute value of the effective porosity as well as a change in slopes $\partial C/\partial \sigma$ and $\partial C/\partial \frac{\Delta p}{\Delta p_{crit}}$ can be observed. This may be understood in view of the fact that in the regime of compressible flow the Mach numbe becomes in general more influencial than the Reynold- number. "urthermore, it can be shown that the experir :tal results are in agreement with analytical predictions ba;ed on the assumption that the flow through the orifices can .e treated like sonic flow th:ough converging nozzles. Details of this analysis are omitted because they wo: ld exceed the purpose of this discussion.

Figures 4-6 through 4-13 indicate that at present merely a limited amount of data is available. However, the change of effective porosity is by its nature primarily important at higher altitudes represented by lower values of σ . Therefore, it may be acceptable at this time to consider merely the effective porosities related to values of $\sigma < 0.5$. With this restriction, the slope $\partial C/\partial \sigma$ versus $\Delta p/\Delta p_{crit}$ has been extracted from Figs 4-6 through 4-9 and is presented in Fig 4-16. It can be seen that the flow through the cloth varies significantly with the pressure differential.

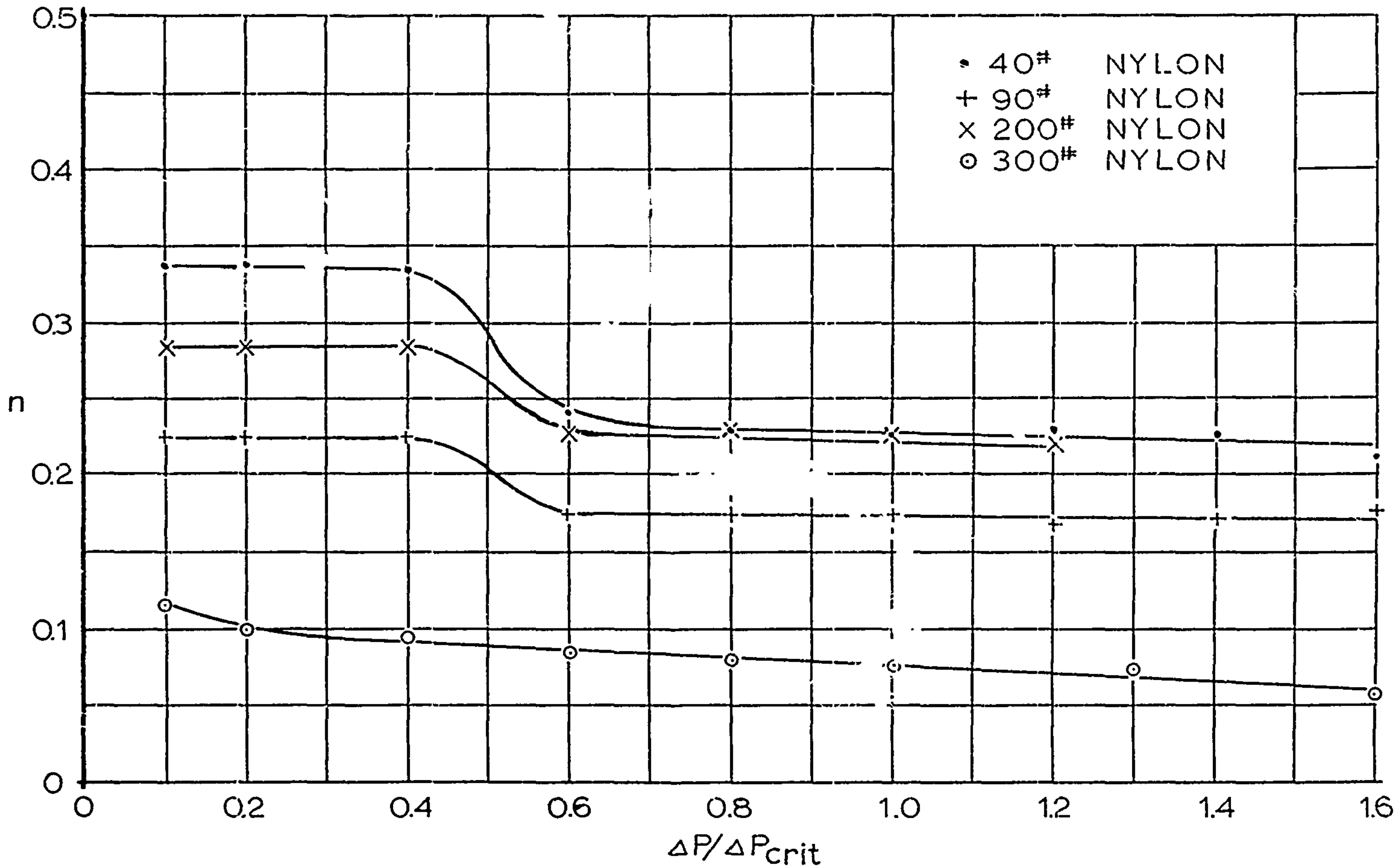

FIG 4-16. EXPERIMENTAL VALUES OF EXPONENT "n" VERSUS PRESSURE RATIO

In the regime of incompressibility, with $\Delta p/\Delta p_{crit}$ between 0.1 and 0.4, some materials indicate a change of slope at relatively high density ratios. This may or may not be related to a change of cloth geometry and this section of the curves is disregarded in the presentation of n versus $\Delta p/\Delta p_{crit}$ in Fig 4-16. In actual cases the effective porosity for this region may be read from Figs 4-6 through 4-9 if necessary.

In summary, this investigation shows that the effective porosity of woven sheets decreases with decreasing density and/or increasing pressure ratio. Figures 4-6 through 4-9 are suitable for a direct reading of the effective porosity for the particular conditions, while Fig 4-16 in connection with equation (4.10) permits the calculation of the effective porosity, C, provided that the related porosity under sea level conditions, C_o, is known.

SECTION 5

SIMPLIFIED TREATMENT OF THE DYNAMICS OF THE OPENING PARACHUTE

5.0 Introduction

The method of the parachute opening shock calculation shown in the present and the preceding editions of the Air Force Parachute Handbook (WADC TR 55-265) provides in general satisfactory results if the approximate filling time is known. However, it must be realized that actually the determination of the filling time is an essential part of the opening shock problem itself, and if the filling time has to be guessed or assumed, the success of the conventional method depends on the personal experience, related information, or the good luck of the parachute engineer.

Several authors (Refs 7, 8, and 18) have proposed strictly analytical methods to calculate the opening time and the opening force. However, in an attempt to make these methods as perfect and as logical as possible, they have become very cumbersome, a number of essential parameters are presently not available and it appears to be very difficult to obtain them with a satisfactory accuracy. The consequence of these circumstances is that those methods have not been reduced to practice and have not been checked out against experimental results. A newer attempt is represented in

Ref 19, however, this method is somewhat specialized for ribbon parachutes and so far has not been reduced to general practice either.

In the following a new analytical method is presented which adopts the concept initially porposed in Ref 7, but includes one basic and simplifying assumption, namely, it is assumed that during the inflation process the drag area of the parachute increases with respect to time in either a linear or simple parabolic manner. On the basis of this assumption a number of governing relationships can be established, and an analytical method has been devised which provides with a reasonable amount of effort numerical values for the filling time as well as a force-time relationship. For a linear relationship, this method is relatively simple, and will be presented in the following sections of this report.

5.1 List of Symbols

a = Speed of sound (ft/sec)

A = Constant = $W x 10^6 / 20\ g \sigma D_o$

B = Constant = $120 (C_D S)_{max} t_f / D_o^3$

c Effective porosity = u/v

C_D = Drag coefficient of parachute

$C_D S$ = Drag area of inflating parachute canopy (ft^2)

d = Diameter of canopy mouth

D = Projected diameter of canopy during inflation (ft)

D_o = Flat diameter of parachute canopy (ft)

g = Acceleration due to Earth's gravity (ft/sec^2)

K = Apparent mass coefficient

L_s = Length of suspension lines (ft)

m_i = Included mass (slugs)

m_a = Apparent mass (slugs)

M = Mach number

p = Atmospheric pressure (lb/ft^2)

p_t = Total pressure (lb/ft^2)

P = Instantaneous opening force (lb)

S = Projected area of canopy during inflation (ft^2)

t_f = Filling time (sec)

T = ratio of instantaneous time to filling time = $= t/t_f$

u = Velocity of flow through canopy roof (ft/sec)

v = Velocity during inflation (ft/sec)

v_{in} = Velocity of flow through canopy mouth (ft/sec)

v_o = Velocity at the beginning of inflation (ft/sec)

V = Canopy volume during inflation (ft^3)

W = Weight of suspended load (lbs)

ρ = Air density ($slugs/ft^3$)

σ = Standard Atmosphere density ratio.

5.2 The Filling Time

The time of inflation of a parachute canopy depends on the mass of air flowing into the canopy and the amount of air which is lost through the porous material of the canopy.

The influx of air depends on the instantaneous relative velocity and the loss of air on the differential pressure, and the inflation of the parachute becomes a matter of a mass balance. The instantaneous velocity as well as the related pressure differential follow from the equation of motion based on Newton's second law. Therefore, one may say that the filling time is a function of the mass balance and the equation of motion.

In addition to these two basic functions, one has to assume a certain idealized shape of the canopy during its inflation. This shape, which was first proposed in Ref 7, is presented in Fig 5-1.

The mass balance can be expressed as

$$\frac{\pi}{4} d^2 V_{in} \rho - \frac{\pi}{2} D^2 U \rho = \frac{d}{dt}(\rho V). \tag{5.1}$$

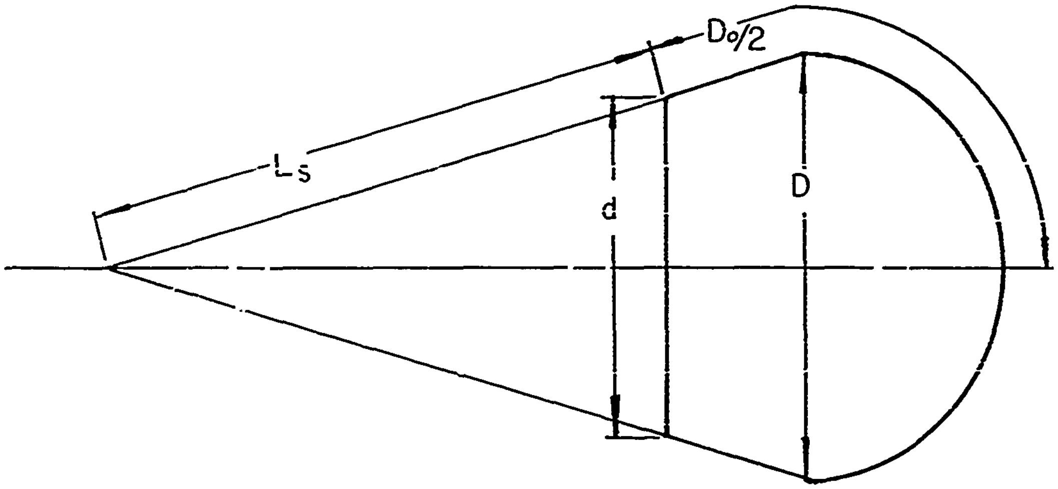

FIG 5-1. IDEALIZED FORM OF THE INFLATING PARACHUTE

As a first approximation, one may assume the velocity-time relationship

$$\frac{V_{in}}{V} = 1 - \frac{t}{t_f} \; . \qquad (5.2)$$

With the symbols as defined in the list of symbols and with the schematic form of the inflating canopy (Fig 5-1), one may establish for the instantaneous projected diameter and the mouth diameter, the relationships

$$D = \frac{2D_o}{\pi} T^{1/2} \qquad (5.3)$$

and

$$d = \frac{\frac{4L_s D_o T^{1/2}}{\pi}}{2L_s + D_o - D_o T^{1/2}} \; . \qquad (5.4)$$

Details of the derivation of these and following terms are shown in Refs 20 and 21.

Substituting these values into equation (5.1) gives

$$v(1-T)t_f \left[\frac{\pi}{4} \left(\frac{\frac{4L_s D_o T^{1/2}}{\pi}}{2L_s + D_o - D_o T^{1/2}} \right)^2 - \frac{2cD_o^2 T}{\pi} \right] = \frac{dV}{dT} \qquad (5.5)$$

The squared term in equation (5.5) represents the diameter of the mouth inlet, which can be simplified if the length of the suspension lines is equal to the nominal diameter, D_o. This simplification gives

$$\frac{\frac{4L_s D_o T^{1/2}}{\pi}}{2L_s + D_o - D_o T^{1/2}} = \frac{\frac{4D_o}{\pi} T^{1/2}}{3 - T^{1/2}} \; . \qquad (5.6)$$

Since the solution of the mass balance incorporates an integration, it is desirable to simplify the term for the inlet diameter further, which could be done satisfactorily with the relationship (Ref 6)

$$d = \frac{2}{\pi} D_o T^{2/3} \tag{5.7}$$

Combining equations (5.5) and (5.7) provides

$$\frac{D_o^2}{\pi} t_f v \left[(1-T)T^{4/3} - 2cT(1-T)\right] = \frac{dV}{dT} \tag{5.8}$$

5.3 The Filling Time in the Infinite Mass Case

If, during the process of inflation, the velocity of the mass-parachute system is nearly constant, equation (5.8) can be simply integrated to obtain

$$t_f = \frac{2D_o}{3\pi v_o (9/70 - c/3)} \tag{5.9}$$

5.4 The Finite Mass Case

The instantaneous velocity of the mass-parachute system varies considerably in the finite mass case; this must be considered in the solution of equation (5.8). The decelerating force in this case is the aerodynamic drag which is primarily developed by the parachute. The mass under deceleration is the suspended weight, the mass of air included in the parachute canopy, and the apparent mass (Ref 22).

From the geometry of the inflating parachute the included mass can be calculated from

$$V = \frac{2D_o^3 T}{\pi}\left\{\left[\frac{1}{4} - \frac{2}{(3-T^{1/2})^3}\right]\sqrt{(3-T^{1/2})^2 - \frac{4T}{\pi^2}} + \frac{T}{\pi}\right\}. \qquad (5.10)$$

In view of a future integration, it is desirable to simplify this form, which can be done in a satisfactory manner by using an approximating parabola (see Ref 21). The included mass then becomes

$$m_i = \frac{2\rho D_o^3}{3\pi^2}\left[1.058 - \frac{\text{[illegible]}}{1.62}\right] \qquad (5.11)$$

The apparent mass is frequently used in theoretical aerodynamics and can be calculated for a few ideal bodies. In general, the apparent mass can be presented in the form as shown in equation (5.12), where K is an experimental factor which for fully inflated solid flat parachutes made out of porous materials is approximately K = 0.25 (Ref 12)

$$m_a = K\pi R^3\rho. \qquad (5.12)$$

During its period of inflation, the parachute will have a varying and different experimental parameter, K, and for the purpose of this simplified method it may be assumed that a satisfactory approximation is

$$K = 0.25T. \qquad (5.13)$$

Combining the diameter-time relationship shown in equation (5.3) and K from equation (5.12), the apparent mass becomes

$$m_a = \frac{\rho D_o^3}{4\pi^2} T^{5/2} . \tag{5.14}$$

Expressing Newton's second law in terms of the suspended weight, the included air, the apparent mass, the aerodynamic drag, and applying certain acceptable simplifications, one obtains the equation of motion

$$2\left[\frac{W \times 10^6}{20 g \sigma D_o^3} + 11.25 T^{3/2}\right]\frac{dv}{dt} + 22.5 v = \frac{20 (C_D S)_{max}\, t_f\, T v^2}{D_o^3} . \tag{5.15}$$

(Details of these simplifications and other operations are given in Ref 20). This equation can be integrated and provides the instantaneous velocity

$$V = \frac{V_o}{\frac{B\, V_o}{2(11.25)^2}\left[(11.25T + A)\ln\frac{11.25T+A}{A} - 11.25T\right] + \frac{11.25T+A}{A}} . \tag{5.16}$$

Substituting the instantaneous velocity in the original mass balance equation, [equation (5.8)], provides a new form of the same equation which can now be used to determine the filling time, t_f:

$$\int_0^{V_{max}} dV = \int_0^1 \frac{\frac{D_o^2 t_f V_o}{\pi}\left[(1-T)T^{4/3} - 2cT(1-T)\right] dT}{\frac{B\, V_o}{2(11.25)^2}\left[(11.25T + A)\ln\frac{11.25T+A}{A} - 11.25T\right] + \frac{11.25T+A}{A}} . \tag{5.17}$$

The right hand side of this equation cannot rigorously be integrated without applying too far reaching simplifications, and a graphical numerical method is recommended.

5.5 Calculation of the Opening Force

The equation of motion [equation (5.15)] can be written in the form

$$\frac{dv}{dt} = \frac{v(22.5+BTv)}{2(A+11.25T)} , \qquad (5.18)$$

where A and B are terms defined in the list of symbols. With $\frac{dv}{dT} = t_f \frac{dv}{dt}$, the force exerted upon the suspended weight is

$$P = \frac{Wv}{2g t_f}\left[\frac{22.5+BTv}{A+11.25T}\right] . \qquad (5.19)$$

By varying T in suitable intervals between 0 and 1, the force-time history of the parachute can now be calculated from equation (5.19) and the maximum force, the so-called opening shock, can be determined.

5.6 Comparison of Experimental and Calculated Values

The determination of opening shock and opening time has been the subject of several experimental efforts, and Ref 10 describes such a study in which parachutes of different types have been investigated with respect to launching velocity and altitude. In view of the experimental information presented in Ref 10, a number of similar cases have been calculated as described in the preceding sections. The results of the experimental (Ref 10) and analytical efforts are presented in Figs 5-2 through 5-7.

A review of these figures indicates that a certain discrepancy exists between experimental and calculated results; however, it will be noted that the order of magnitude of the numerical values as well as the principal trends of the phenomena appear to be in agreement.

One situation makes a comparison very difficult, namely, the experimental results are all related to the launching velocity while the calculation of the opening times and opening forces begins with the instantaneous velocity of the system when the parachute begins to inflate. For the purpose of comparison, it was therefore necessary to calculate for the cases presented in Ref 10 the velocity at the instance of parachute inflation. This velocity was then used as the initial velocity for the analytical determination of the filling time and the opening force. In view of the uncertainty which necessarily exists in the calculation of such an assumed velocity increment, one must consider the basis of comparison between experimental and analytical results as not completely satisfactory. A shift of the respective curves can improve or deteriorate the agreement presented in the Figs 5-2 through 5-7. In general, however, it appears that the presented analytical method is a workable one and that the results appear to bear some real significance.

Further efforts are now being made in which the

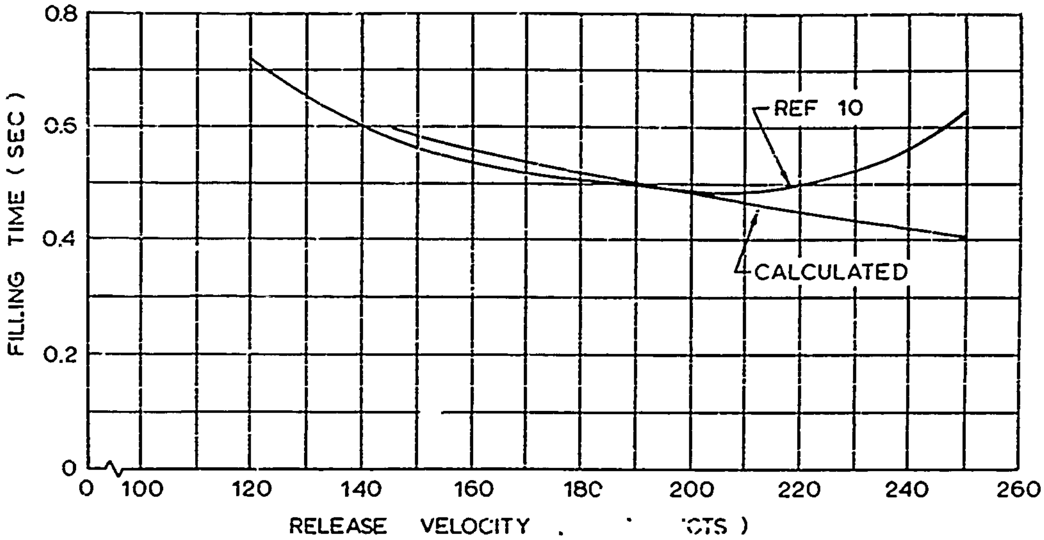

FIG 5-2. COMPARISON OF EXPERIMENTAL AND CALCULATED VALUES OF FILLING TIME FOR A 28 FT. FLAT CIRCULAR PARACHUTE AT AN ALTITUDE OF 7,000 FT

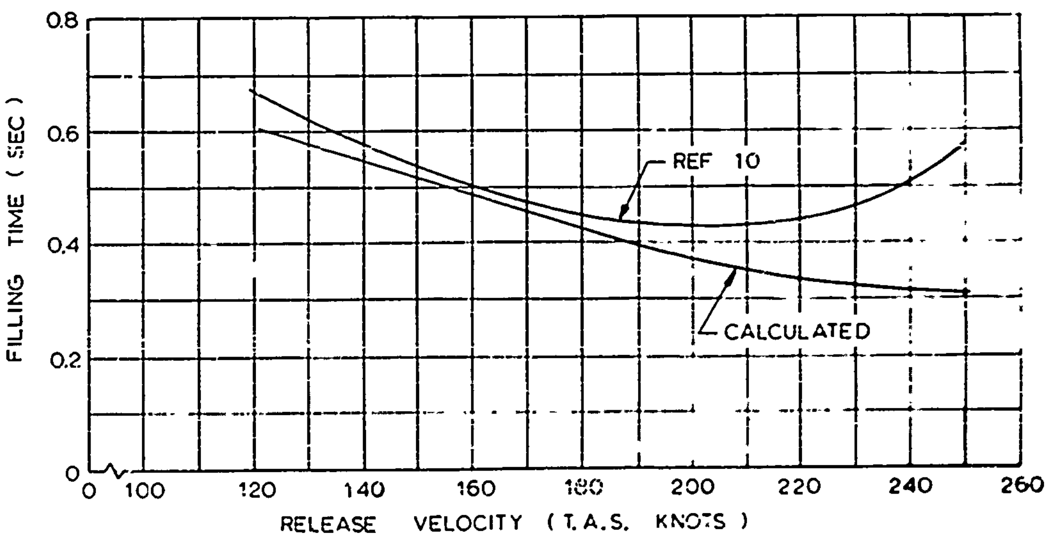

FIG 5-3 COMPARISON OF EXPERIMENTAL AND CALCULATED VALUES OF FILLING TIME FOR A 28 FT FLAT CIRCULAR PARACHUTE AT AN ALTITUDE OF 14,000 FT

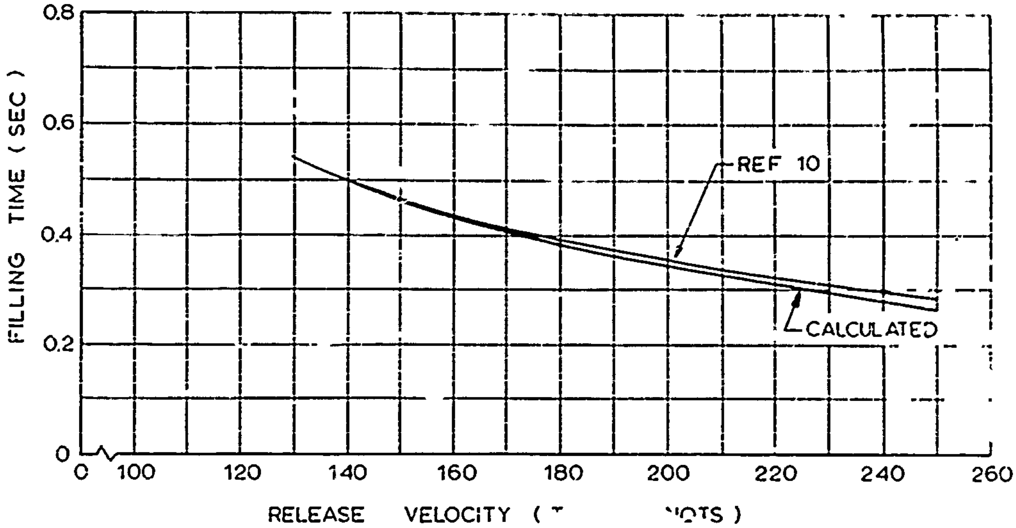

FIG 5-4. COMPARISON OF EXPERIMENTAL AND CALCULATED VALUES OF FILLING TIME FOR A 28 FT FLAT CIRCULAR PARACHUTE AT AN ALTITUDE OF 20,000 FT

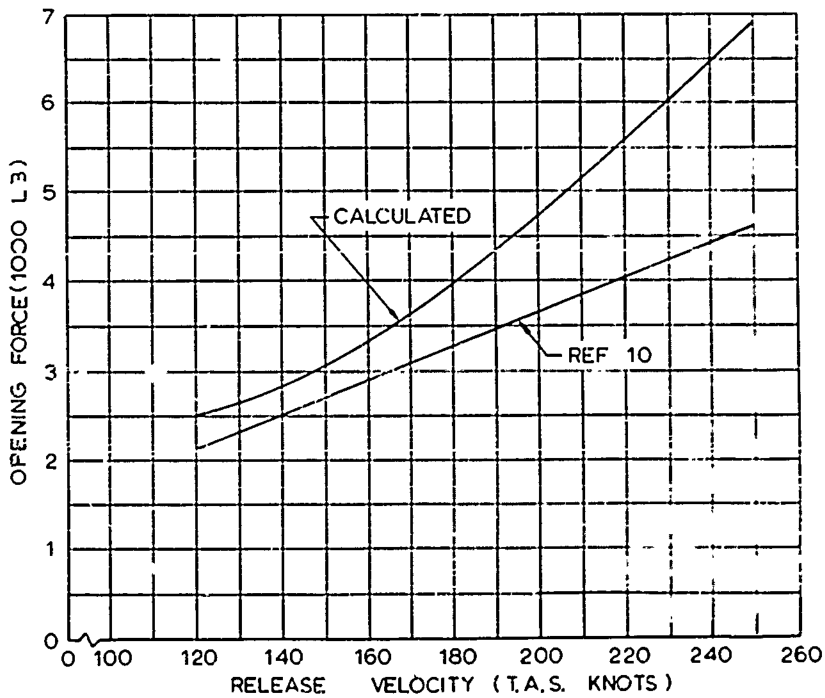

FIG 5-5. COMPARISON OF EXPERIMENTAL AND CALCULATED VALUES OF OPENING FORCE FOR A 28 FT FLAT CIRCULAR PARACHUTE AT 7,000 FT

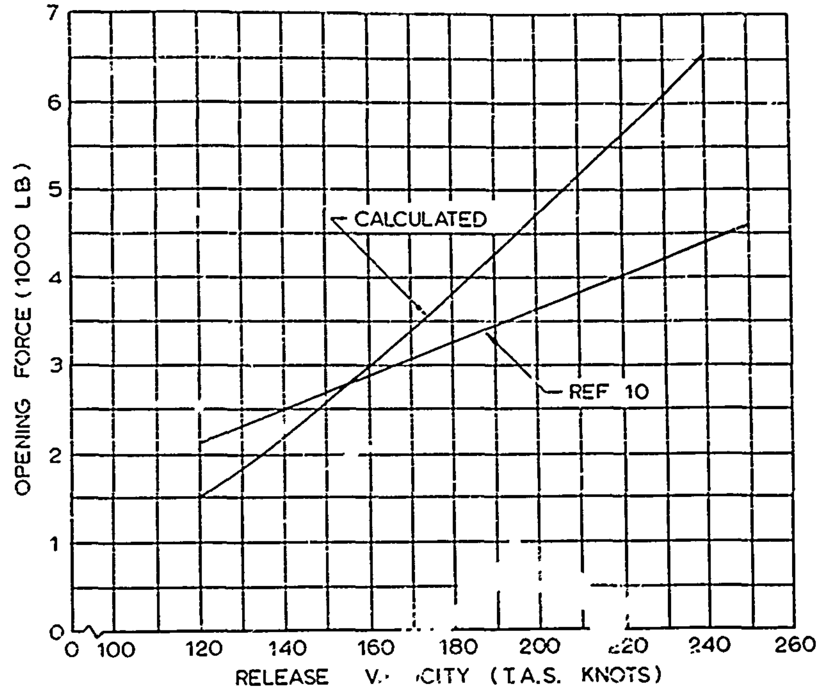

FIG 5-6. COMPARISON OF EXPERIMENTAL AND CAL- CULATED VALUES OF OPENING FORCE FOR A 28 FT FLAT CIRCULAR PARACHUTE AT 14,000 FT

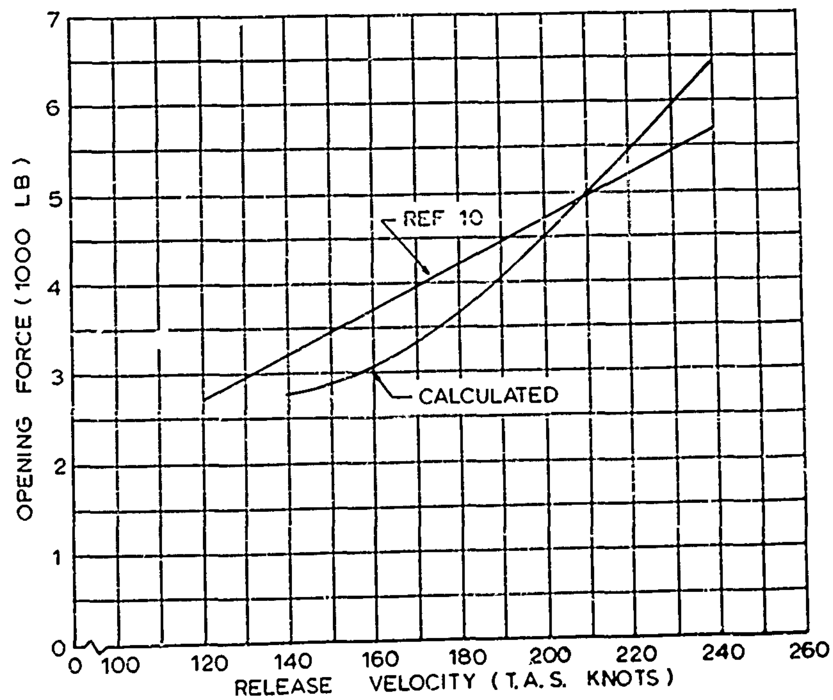

FIG 5-7. COMPARISON OF EXPERIMENTAL AND CAL- CULATED VALUES OF OPENING FORCE FOR A 28 FT FLAT · CIRCULAR PARACHUTE AT 20,000 FT

numerical results of the analytical method based on a parabolic increase of drag area versus time will be compared with experimental evidence. In addition, the validity of the experimental data in view of its value as basis of comparison is under investigation.

SECTION 6

MODIFICATION OF THE OPENING SHOCK CHARACTERISTICS OF PARACHUTES

The classical problem of a parachute application is to reduce the launching speed of the suspended load to its equilibrium velocity in a relatively short time with a moderate maximum force.

An analysis of the filling process indicates that in the initial phase of inflation, most parachutes assume the shape of a slender truncated cone, capped by a hemisphere. During this phase, the inflation progresses very slowly and the retarding force is relatively low. The maximum force, the so-called opening shock, occurs when the parachute has attained approximately 2/3 of its final size.

The slow progress of inflation at its early phase is partially due to a certain venturi effect established by the in- and outflow of air through the small base area of the cone and the vent hole in the apex as well as through the cloth itself In order to reduce the filling time without causing an increase of the opening shock, it was theorized that it might be possible to reduce the venturi effect by means of an obstruction in the inlet area, which would tend to develop locally higher pressure and thereby promote a spreading of the lower rim of the canopy which in turn would expedite the filling of the parachute. With the proper form, size, and location of this obstruction it appears possible to shorten the initial, time-wasting phase of the inflation without affecting the maximum opening force, which occurs at a later instant.

It is apparent that this method would be particularly effective with parachutes which have a relatively long initial phase of inflation.

In order to check these speculations, wind tunnel experiments were made in which a large primary parachute was suspended, and as obstruction a much smaller parachute was arranged in its mouth area. Initially both parachutes were reefed, and after attaining the desired air velocity, both parachutes were disreefed. The opening force and rate of inflation of both parachutes was recorded. Figures 6-1 and 6-2 show the general arrangement and the reproducibility of the force-time history, respectively.

After some exploratory experiments, a certain optimum arrangement concerning size and location of the secondary parachute was established. The principal effect of the modification can be seen in Figs 6-3 and 6-4. One recognizes that by means of the secondary parachute the entire opening process is accomplished in a shorter time with out significant increase of the opening force.

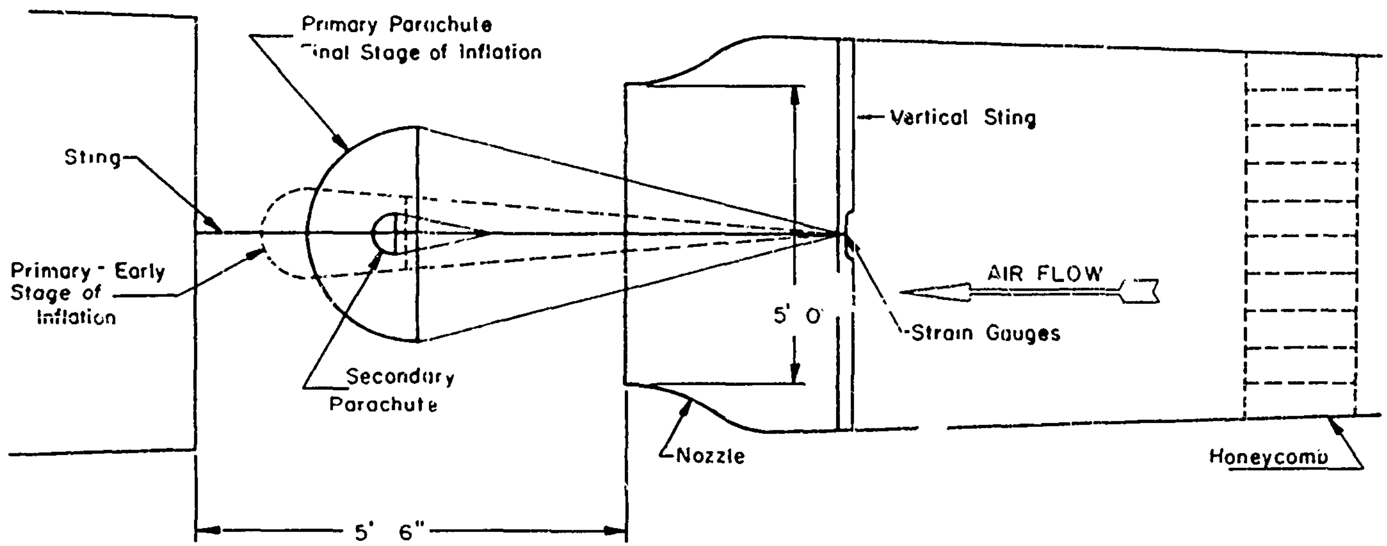

FIG 6-1. TEST SECTION AND ARRANGEMENT FOR OPENING SHOCK STUDIES (INFINITE MASS CASE)

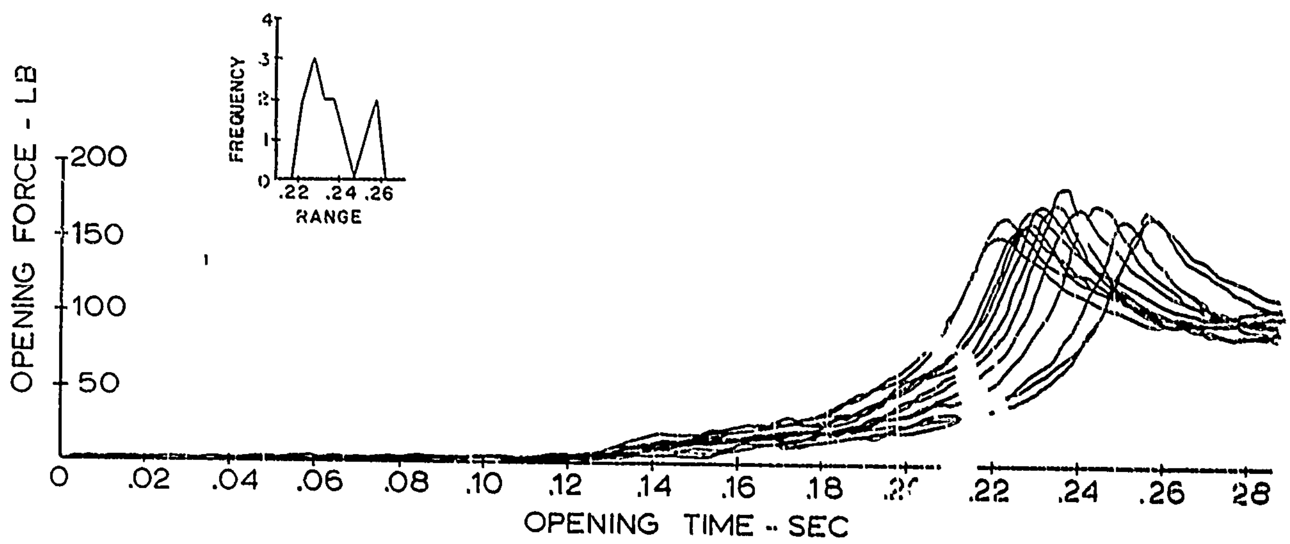

FIG 6-2. OPENING FORCE-TIME HISTORIES OF A CIRCULAR FLAT PRIMARY PARACHUTE ALONE

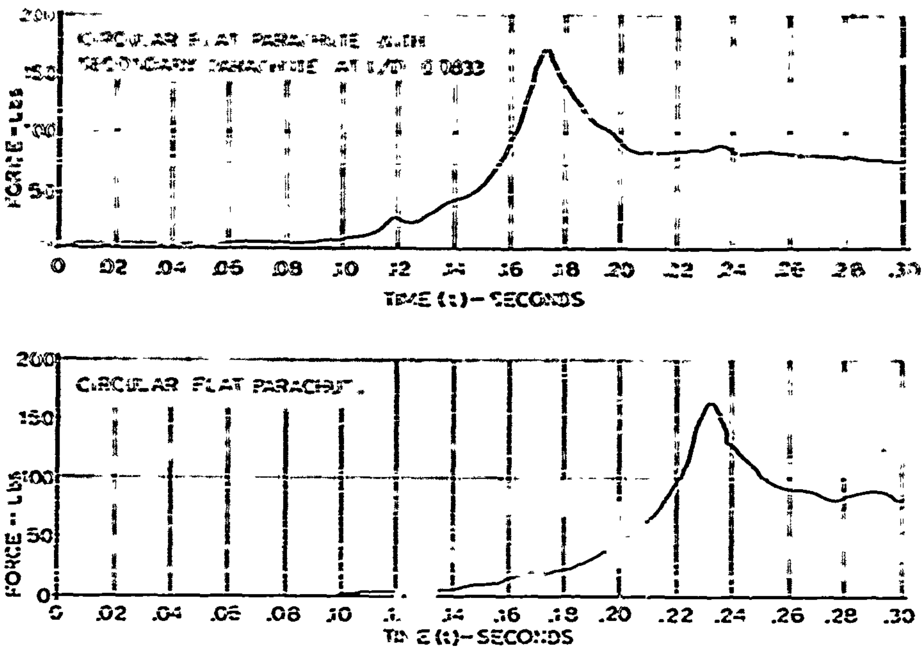

FIG 6-3. INFLATION CHARACTERISTICS OF A SOLID FLAT PARACHUTE WITH AND WITHOUT SECONDARY PARACHUTE

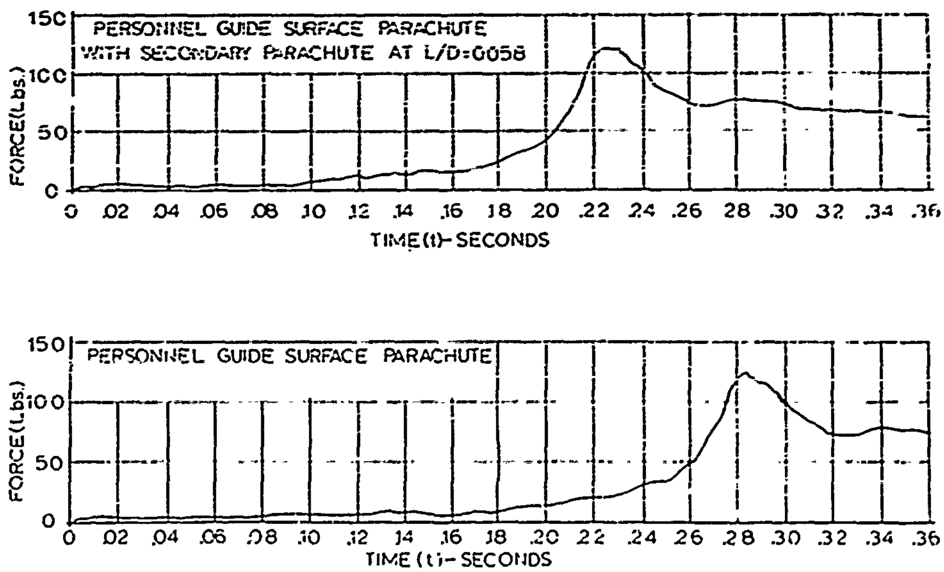

FIG 6-4. INFLATION CHARACTERISTICS OF A PERSONNEL GUIDE SURFACE PARACHUTE WITH AND WITHOUT SECONDARY PARACHUTE

More complete information concerning the characteristics and effectiveness of the system is given in Figs 6-5 and 6-6. It can be seen, for example, that for the personnel guide surface parachute, which has a particularly long initial phase, the opening time has been reduced to 68% of the value of the unmodified parachute, while the opening force has been increased by only 3%.

Figure 6-7 illustrates the force-time history of both the primary and the secondary parachutes. We see that the maximum force of the secondary parachute amounts to about 3% of that of the primary parachute. Furthermore, it has been observed and confirmed by the force recordings that the secondary parachute collapses when the primary parachute approaches its final size.

In view of the importance of the indicated tendencies, drop tests were made as soon as sufficient laboratory data was available, and so far the expectations based on the wind tunnel studies have been satisfactorily confirmed (Ref 23). In these experiments, the parachutes were standard items. Only through the addition of a small secondary parachute did the originally slower opening guide surface parachute inflate faster than a comparable but unmodified circular flat parachute. The opening force was insignificantly affected.

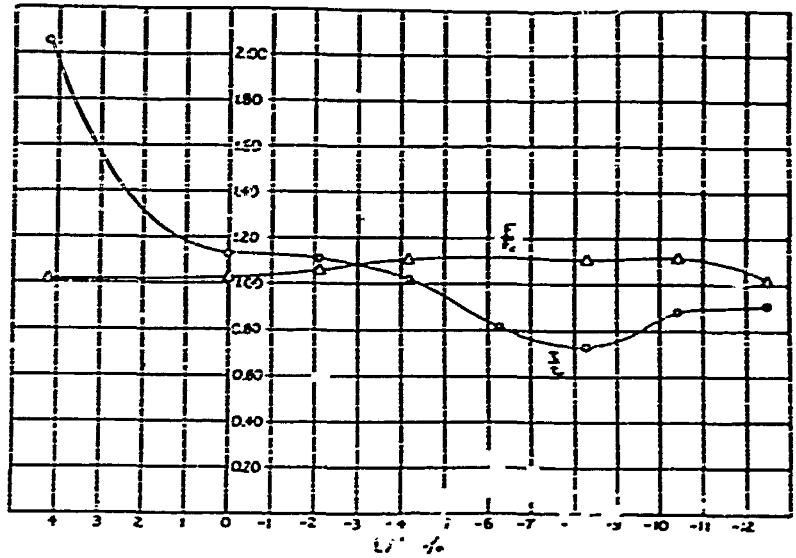

FIG 6-5. OPENING TIME AN[illegible] OPENING FORCE VERSUS LOCATION OF THE SE[illegible]ONDARY PARACHUTE FOR A CIRCULAR F[illegible]AT PRIMARY PARACHUTE

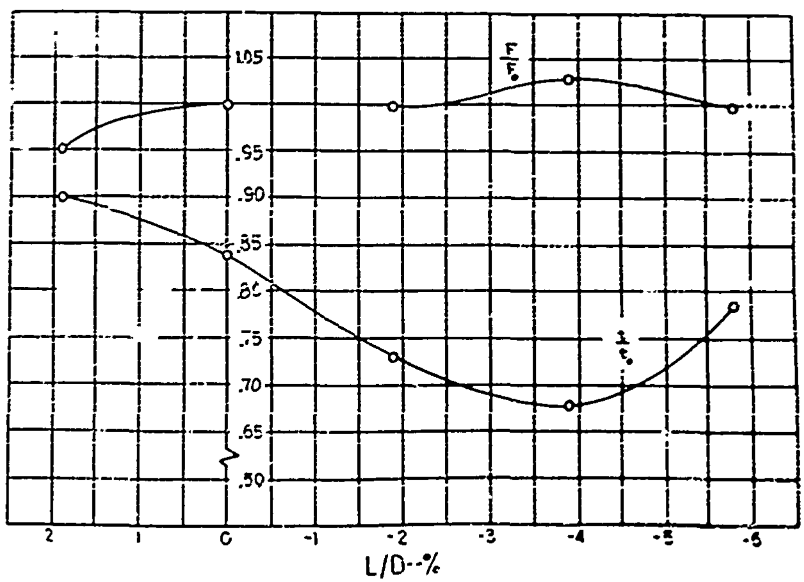

FIG 6-6. OPENING TIME AND OPENING FORCE VERSUS LOCATION OF THE SECONDARY PARACHUTE FOR A PERSONNEL GUIDE SURFACE PRIMARY PARACHUTE

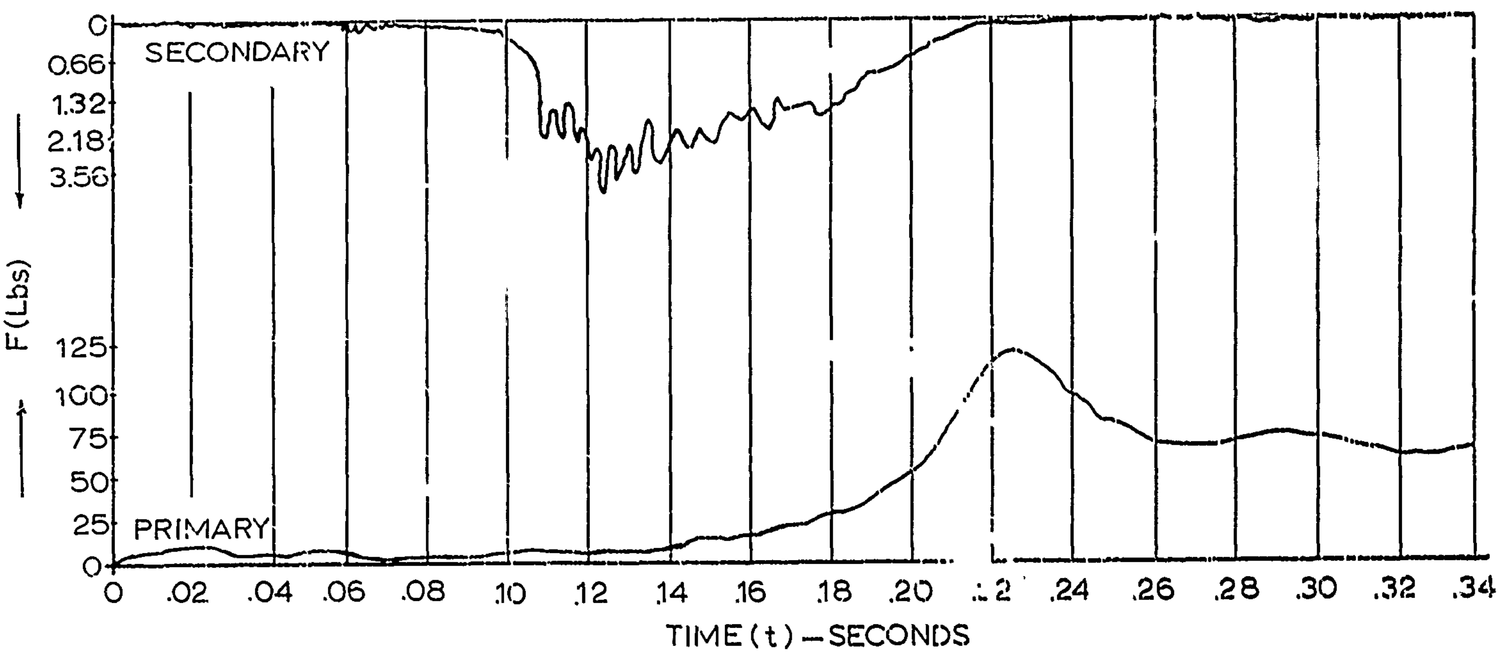

FIG 6-7. OPENING FORCE VERSUS TIME OF A PERSONNEL GUIDE SURFACE PRIMARY PARACHUTE AND A CIRCULAR FLAT SECONDARY PARACHUTE

REFERENCES

1. Schlichting, H.: Boundary Layer Theory, McGraw-Hill, New York, 1955.

2. Swain, Miss L. W.: Turbulent Wake Behind a Body of Revolution, Proceedings of the Royal Society of London, Ser. A, Vol. 125, 1929.

3. Heinrich, H. G. and Riabokin, T.: Analytical and Experimental Considerations of the Velocity Distribution in the Wake of a Body of Revolution, WADC Technical Report No. 60-257, December, 1959.

4. Goldstein, S.: On the Velocity and Temperature Distribution in the Turbulent Wake Behind a Heated Body of Revolution, Proceedings of the Cambridge Philosophical Society, Vol. 34, 1938, pp. 48-67.

5. Hall, A. A. and Hislop, G. S.: Velocity and Temperature Distributions in the Turbulent Wake Behind a Heated Body of Revolution, Proceedings of the Cambridge Philosophical Society, Vol. 34, pp. 345-353.

6. Ballinger, J. G., and Parks, J. W.: Aerodynamic Characteristics of Blunt Bodies Immersed in Wake Flow, University of Minnesota, Institute of Technology, Rosemount Aeronautical Laboratories, Research Report No 165, October, 1959.

7. O'H...a, F.: Notes on the Opening Behavior and the Opening Forces of Parachutes, Royal Aeronautical Society Journal, November, 1949.

8. Foote, J. R., and Scherberg, M. G.: Dynamics of the Opening Parachute, Proceedings of the Second Midwestern Conference on Fluid Dynamics, Ohio State University, 1952.

9. Hallenbeck, G. A.: The Magnitude and Duration of Parachute Opening Shocks at Various Altitudes, and Air Speeds, AF Memorandum Report [illegible]9-696-6S, 1944.

10. Freeman, Henry F. and [illegible]senberg, I.: High Altitude and High Air Speed Tests of Standard Parachute Canopies, AFFTC TR 58-32, ASTIA Document No AD 152 286.

11. Karman, T.: Note on Analysis of the Opening Shock of Parachutes at Various Altitudes, Army Air Corps Scientific Advisory Group, 1945.

12. Heinrich, H. G.: Experimental Parameters in Parachute Opening Theory, Bulletin of the 19th Symposium on Shock and Vibration, 1953, Office of the Secretary of Defense, Washington, D.C.

13. Heinrich, H. G.: Drag and Stability of Parachutes, IAS Eng Review, June, 1956.

14. Heinrich, H. G. and Haak, E. L.: Stability and Drag of Parachutes with Varying Effective Porosity (in preparation for printing).

15. Eckert, B. and Pfluger, F.: The Resistance Coefficient of Commercial Round Wire Grids, NACA TM 1003, January, 1942.

16. Hoerner, S. F.: Aerodynamic Drag (Published by author), 1958.

17. Schubauer, G. B., Spangenburg, W. G., and Klebanoff, P.S.: Aerodynamic Characteristics of Damping Screens, National Bureau of Standards, NACA TN [illegible] January, 1950.

18. Weinig, Friedrich S.: On the Dynamics of the Opening Shock of a Parachute, USAF OAR TR 6, 1951.

19. Wilcox, Bruce: The Calculation of Filling Time and Transient Loads for a Parachute Canopy During Deployment and Opening, Sandia Corporation SC-4151 (TR), February, 1958.

20. Progress Report No 12, Theoretical Parachute Investigations, Department of Aeronautical Engineering, University of Minnesota.

21. Cutshall, Richard C.: Analytical Investigations of Parachute Inflation Time, Master Thesis, June 1959, University of Minnesota.

22. Streeter, Victor L.: Fluid Dynamics, McGraw-Hill Company, 1948.

:cut,